

1 **Abstract**

2 There is growing interest in the formation of secondary organic aerosol (SOA) through
3 condensed aqueous phase reactions. In this study, we use a global model (IMPACT) to
4 investigate the potential formation of SOA in the aqueous phase. We compare results
5 from several multiphase process schemes with detailed aqueous phase reactions to
6 schemes that use a first order gas-to-particle formation rate based on uptake coefficients.
7 The predicted net global SOA production rate in cloud water ranges from 13.1 Tg/yr to
8 46.8 Tg/yr while that in aerosol water ranges from -0.4 Tg/yr to 12.6 Tg/yr. The predicted
9 global burden of SOA formed in the aqueous phase ranges from 0.09 Tg to 0.51 Tg. A
10 sensitivity test to investigate two representations of cloud water content from two global
11 models shows that increasing cloud water by an average factor of 2.7 can increase the net
12 SOA production rate in cloud by a factor of 4 at low altitudes (below approximately 900
13 hPa). We also investigated the importance of including dissolved iron chemistry in cloud
14 water aqueous reactions. Adding these reactions increases the formation rate of aqueous
15 phase OH by a factor of 2.6 and decreases the amount of global aqueous SOA formed by
16 31%. None of the mechanisms discussed here is able to provide a best fit for all
17 observations. Rather, the use of an uptake coefficient method for aerosol water and a
18 multi-phase scheme for cloud water provides the best fit in the Northern Hemisphere and
19 the use of multiphase process scheme for aerosol and cloud water provides the best fit in
20 the tropics. The model with iron chemistry under predicts oxalate measurements in all
21 regions. Finally, the comparison of O/C ratios estimated in the model with those
22 estimated from measurements shows that the modeled SOA has a slightly higher O/C
23 ratio than the observed SOA for all cases.

1 **1. Introduction**

2 Secondary organic aerosol (SOA) has been shown to be an important component of non-
3 refractory submicron aerosol in the atmosphere (Zhang et al., 2007; Jimenez et al. 2009).
4 SOA is known to form from the gas/particle partitioning of semi-volatile organic
5 compounds produced by gas phase photochemistry (Pankow, 1994; Odum et al., 1996).
6 However, models that only include this SOA formation mechanism typically
7 underestimate the SOA mass as well as the oxygen-to-carbon (O/C) ratio (e.g., DeGouw
8 et al., 2005; Heald et al., 2005; Volkamer et al., 2006; Dzepina et al., 2009). In addition,
9 the observed O/C ratios in aged ambient organic aerosol (OA) cannot be explained using
10 measured O/C ratios in dry smoke chamber experiments (Aiken et al. 2008; Ng et al.,
11 2010). One method that has been used to help close the gap between measured and
12 modeled SOA is to use a refined treatment for primary organic aerosol (POA) that allows
13 them to evaporate and further oxidize (Robinson et al. 2007; Pye and Seinfeld, 2010;
14 Hodzic et al., 2010; Lee-Taylor et al., 2011). However, there are large uncertainties in
15 how to treat the evaporation rate as well as the oxidation mechanism for POA and thus
16 the SOA yield from this source (Pye and Seinfeld, 2010; Spracklen et al. 2011).

17 Aqueous phase processing, as a complementary pathway to gas/particle partitioning of
18 semi-volatile and low volatility gases, has the potential to enhance both SOA mass and
19 the O/C ratio in atmospheric OA. Water-soluble and polar gases are taken up by the
20 aqueous phase and can be oxidized in water thereby leading to the production of low
21 volatility substances (e.g., organic acids and especially their corresponding salts,
22 oligomers, and organosulfates) (Blando and Turpin, 2000; Warneck, 2003; Liggio et al,
23 2005; Sorooshian et al., 2007; Tan et al., 2009). These low-volatility products

1 predominately stay in the particle phase after water evaporation (Blando and Turpin,
2 2000; El Haddad et al., 2009) and tend to have higher O/C ratios than those that form in
3 gas phase reactions (Herrmann et al., 2005; Lim et al., 2010; Ervens and Volkamer,
4 2010). This is because the precursors for the aqueous phase reactions tend to be small
5 compounds with low-molecular weight (MW) that already have high O/C ratios, and the
6 aqueous oxidation of these small compounds either tends to add O-containing functional
7 groups to C-C bonds (thereby forming higher O/C ratio dicarboxylic acids) or to react
8 with themselves to keep the same carbon structure and the same O/C ratio (thereby
9 forming oligomers) (Ervens et al., 2011).

10 Laboratory studies have shown that aqueous phase reactions can produce SOA from C2
11 and C3 carbonyl compounds including glyoxal, methylglyoxal, glycolaldehyde, pyruvic
12 acid and acetic acid (Ervens et al., 2003; Carlton et al., 2006, 2007; Altieri et al., 2008;
13 Perri et al., 2009; Tan et al., 2009, 2010, 2012; Lim et al. 2010). The major products from
14 the oxidation of these carbonyl compounds are carboxylic acids, of which the most
15 abundant is oxalic acid. Oxalic acid is also observed to be part of the aerosol emitted in
16 biomass burning (Kundu et al., 2010) and is observed to be formed from the
17 photochemical ageing of OA (Eliason et al., 2003). In contrast to reactions in cloud water,
18 the major products formed from the reactions of C2 and C3 carbonyl compounds in
19 aerosol water are oligomers (Ervens and Volkamer, 2010; Lim et al., 2010).

20 Several models to date have been developed to estimate the amount of SOA formed in
21 the aqueous phase (denoted aqSOA hereafter). Chen et al. (2007) used a box model to
22 investigate the formation of SOA from aqueous phase reactions in cloud water using an
23 explicit aqueous mechanism that included organic acid formation from glyoxal and

1 methylglyoxal; they found that aqueous phase processing increased the SOA
2 concentration by 27% for a rural scenario and by 7% for an urban scenario. Carlton et al.
3 (2008) used a simplified mechanism with a fixed yield of 4% for the conversion of
4 glyoxal to aqSOA in a regional air quality model. The model's ability to predict the
5 concentration of water soluble organic carbon (WSOC) from aircraft measurements over
6 northeastern US was improved and the bias between predicted SOA mass and
7 observations was decreased from -64% to -15%. Myriokefalitakis et al. (2011) and Liu et
8 al. (2012) employed a global model to study the formation of SOA in clouds and found
9 that the global production rate could be 13-30 Tg/yr. The contribution of aerosol water to
10 the formation of aqueous phase SOA from glyoxal and methylglyoxal has also been
11 estimated in global models (Fu et al., 2008, 2009; Stavrakou et al., 2009; Lin et al.,
12 2012). The amount of irreversible uptake of glyoxal and methylglyoxal into aerosol water
13 was predicted to be much smaller than that in cloud droplets, when the same reactive
14 uptake parameter ($\gamma=2.9\times10^{-3}$) was used (Fu et al., 2008, 2009). This result was
15 confirmed by Lin et al. (2012) using the same basic approach. Stavrakou et al. (2009),
16 however, concluded that the source of SOA over the continents from uptake of glyoxal
17 by aerosol particles was at least as large as that from cloud droplets or even up to 60%
18 larger. These authors implemented an in-cloud formation parameterization similar to
19 Ervens et al. (2008) rather than using an uptake formation scheme as in Fu et al. (2008,
20 2009) and Lin et al. (2012).

21 Uncertainties in the formation of aqSOA stem from uncertainties in how to treat its
22 formation rate. The use of a single reactive uptake parameter γ in aqSOA formation as in
23 Fu et al. (2008, 2009) and Lin et al. (2012) implies a surface-limited uptake process, but

1 Ervens and Volkamer (2010) found no correlation between the SOA volume increase and
2 the seed aerosol surface area for most of seed aerosols used the laboratory study by
3 Volkamer et al. (2009). Instead, the SOA volume increase was shown to be linear to the
4 total water mass on these seed particles, implying that SOA was formed as a result of a
5 bulk process. On the other hand, the positive correlation between the SOA volume
6 increase and the surface area observed for mixed sulfate/fulvic acid seed particles in the
7 study by Ervens and Volkamer (2010) suggests that a surface process dominated the
8 formations on these mixed particles. Waxman et al. (2013) also found that a surface
9 limited uptake process could explain the observed gas-phase glyoxal mass in Mexico
10 City. Finally, the use of an identical reactive uptake parameter for both cloud droplets and
11 aerosol water, as in Fu et al. (2008) does not account for differences in the chemistry of
12 carbonyl compounds between cloud water and aerosol water (Lim et al., 2010; Ervens
13 and Volkamer, 2010).

14 Other uncertainties in treating the formation of aqSOA include the treatment of aqueous
15 chemistry as well as the amount of cloud water represented in a model. Iron chemistry in
16 cloud water has been shown to be a major source of aqueous OH (Ervens et al., 2003;
17 Deguillaume et al., 2005), which is known to initiate the oxidation of glyoxal and
18 methylglyoxal. However, no model, to our knowledge, has included the oxidation of iron
19 in simulating the formation of aqSOA in cloud water. In addition, the amount of cloud
20 water in a model can influence SOA production rates (Liu et al. 2012; He et al., 2013).

21 In this paper, we focus on the aqueous formation of SOA from C2 and C3 carbonyl
22 compounds not only because they are highly water soluble but also because most of the
23 existing laboratory studies use these compounds as surrogates to examine aqueous SOA

1 formation, so that sufficient information exists to derive their reaction mechanisms. We
2 use a 3-D chemical transport model to test three representations of aqueous chemistry
3 leading to SOA formation: two detailed mechanisms using explicit multi-phase
4 gas/aqueous phase chemical mechanisms and a parameterized surface-limited uptake
5 mechanism using a reactive uptake parameter γ to simulate the formation of aqSOA in
6 both cloud water and aqueous aerosol water. We also examine the use of aqueous iron
7 chemistry in cloud water and the effect of changing the cloud water amount within the
8 model.

9 This paper is organized as follows. The model and chemistry are described in Sect. 2.
10 Global budgets and distributions of aqSOA predicted from a base mechanism are
11 analyzed in Sect.3. The change in global budgets of aqSOA resulting from four other
12 mechanisms and one different cloud field are also analyzed in Sect. 3. We compare the
13 simulations with available measurements in Sec. 4. Finally Sect. 5 summarizes our
14 conclusions.

15 **2. Model description**

16 We used the IMPACT chemical transport model (Penner et al., 1998; Liu and Penner,
17 2002; Liu et al., 2005; Ito et al., 2007; Feng et al., 2007; Wang et al., 2009; Xu and
18 Penner, 2012; Lin et al., 2012) to simulate the formation of SOA. The IMPACT model
19 includes the microphysics of sulfate aerosol and the interactions between sulfate and non-
20 sulfate aerosols based on the aerosol module developed by Herzog et al. (2004) (Liu et
21 al., 2005). Some versions include the formation of nitrate and ammonium aerosols as
22 well, but here, we extended the sulfate microphysics module initially described by Liu et

1 al. (2005) to include the formation of SOA (Lin et al., 2012). SOA is assumed to have a
2 log-normal size distribution with a mode radius of 0.0774 μm and a geometric standard
3 deviation of 1.402. It becomes mixed with sulfate through the condensation of gas phase
4 sulfuric acid, through coagulation with pure sulfate aerosols, and through aqueous
5 formation of sulfate. We used the 1997 meteorological fields from the National
6 Aeronautics and Space Administration (NASA) Data Assimilation Office (DAO) GEOS-
7 STRAT model (Coy and Swinbank, 1997; Coy et al., 1997) as input to the chemical
8 transport model. The meteorology was defined on a 4° latitude x 5° longitude horizontal
9 grid with 46 vertical layers. Cloud water content was not available from the
10 meteorological fields, and thus was diagnosed with a parameterization used in the NCAR
11 CCM2 model (Hack, 1998). The large scale stratiform cloud fraction was determined
12 based on the grid box mean relative humidity (RH) as calculated from the DAO
13 meteorological data using the parameterization by Sundqvist et al. (1989). The
14 convective cloud fraction was parameterized by using the convective mass flux (Xu and
15 Krueger, 1991). The model was run for a 1-year time period with a 1-month spin up time.
16 Global emissions of gases, aerosols and aerosol precursors and treatments of dry and wet
17 deposition used here are the same as those used in Lin et al. (2012).

18 **2.1. SOA formation through gas-particle partitioning in the gas phase**

19 In this paper, we adopted the gas-particle partitioning mechanism for SOA formation
20 described by Lin et al. (2012). Lin et al. (2012) use a fully explicit gas-phase
21 photochemical mechanism to predict the formation of semi-volatile organic compounds
22 (SV-VOCs) which then partition to an aerosol phase. These condensed SV-VOCs were
23 assumed to further undergo aerosol phase reactions to form oligomers with an assumed

1 time constant (nominally 1 day). In addition, we also accounted for SOA formation due
2 to heterogeneous reactions of epoxides on the surface of wet sulfate aerosol by assuming
3 an uptake coefficient of 0.0029, the value measured for glyoxal by Liggio et al. (2005).
4 Lin et al. (2012) explored the effect of OH recycling in the oxidation of isoprene on the
5 formation of SOA using three different gas-phase chemical mechanisms. Here, we used
6 Simulation C in Table 1 in Lin et al. (2012), since this mechanism was shown to best
7 capture the observations of OH and the first generation products of isoprene-OH
8 reactions. The mechanism includes the formation of epoxide proposed by Paulot et al.
9 (2009), while HO_x regeneration followed Peeters et al. (2009) but with a reduced rate for
10 the 1,5-H and 1,6-H shifts in isoprene radicals by a factor of 10. The basic
11 photochemistry of O₃, OH, NO_x and the oxidation of other VOCs utilized the chemical
12 mechanism published by Ito et al. (2007).

13 **2.2. SOA formation in the aqueous phase**

14 In the presence of cloud droplets or aqueous particles, water-soluble gases (e.g., glyoxal,
15 methylglyoxal, and glycolaldehyde) will dissolve in the aqueous phase and be further
16 oxidized by OH and NO₃ radicals to form products with lower volatility (e.g.,
17 dicarboxylic acids and oligomers) (Ervens et al., 2011; Lim et al., 2010). These low
18 volatility products are assumed to remain entirely in the particulate phase as SOA, when
19 water is evaporated. In this paper, five aqSOA components are predicted: glyoxylic acid,
20 pyruvic acid, oxalic acid, and two classes of oligomers formed from glyoxal and
21 methylglyoxal.

1 **2.2.1. Multiphase reaction scheme**

2 The change of aqueous and gas phase species due to the photochemical reactions and the
3 exchange between the gas and aqueous phase are expressed by the following equations,

$$\frac{dC_g}{dt} = P_g - (L_g + k_t Q)C_g + \frac{k_t}{HRT} C_a \quad (1a)$$

$$\frac{dC_a}{dt} = P_a + k_t Q C_g - (L_a + \frac{k_t}{HRT}) C_a \quad (1b)$$

4 Where C_a and C_g are aqueous and gas phase concentrations (molecules cm^{-3} air), P_a and
5 P_g are aqueous and gas phase chemical production rates (molecules cm^{-3} air s^{-1}), L_a and L_g
6 are aqueous and gas phase pseudo-first-order chemical loss rates (s^{-1}), H is the Henry's
7 law coefficient (M atm^{-1}), R is the universal gas constant ($\text{L atm mol}^{-1}\text{K}^{-1}$), T is the
8 temperature (K), Q is the liquid water content ($\text{cm}^3 \text{H}_2\text{O cm}^{-3}$ air), and k_t ($\text{cm}^3 \text{air cm}^{-3}$
9 $\text{H}_2\text{O s}^{-1}$) is a first-order rate constant that represents diffusion through the gas phase and
10 across the interface of the drop (see Schwartz (1986) and Lelieveld and Crutzen (1991)
11 for details).

12 We used the method described by Sillman et al. (2007) to solve Eq. (1a) and (1b). This
13 method is based on the implicit (reverse Euler) equations but incorporates a number of
14 nonstandard treatments as described in Sillman (1991) and Barth et al. (2003). The mass
15 transfer rate across the gas-aqueous interface is assumed to be limited by diffusion and is
16 determined for each gas by its molecular diffusion, mass accommodation coefficient and
17 Henry's law constant (Lelieveld and Crutzen, 1991). Since not all gas diffusivities are
18 known, we used a single gas diffusivity of $0.1 \text{ cm}^2 \text{s}^{-1}$ for all gaseous species. This is
19 unlikely to add a large uncertainty since the values of available gas diffusivities do not

1 differ by much from the value we used here (Schwartz, 1986; Lelieveld and Crutzen,
2 1991). Accommodation coefficients for each species are listed in Table S7 in the
3 Supplement and assumed to be 0.05 for species for which no information is available. For
4 situations in which the average concentration of an aqueous species is limited by the rate
5 of diffusion within the aqueous phase, the average aqueous phase concentration is scaled
6 to the surface concentration by the factor Q as shown in Eq. 2.14 in Lelieveld and
7 Crutzen (1991). In addition, an effective cloud droplet radius of $10 \mu\text{m}$ is assumed for all
8 clouds, while the effective radius for aqueous sulfate particles (the ratio of third to second
9 moment of the wet sulfate aerosol size distributions) is calculated explicitly according to
10 their relative humidity-dependent size distribution. Aerosol water was calculated based
11 on the amount of water uptake for the modeled pure sulfate particles, which is based on
12 the equilibrium Köhler theory (Ghan and Zaveri, 2007) using the RH and hygroscopicity
13 of sulfate to calculate the wet volume mean radius from the dry volume mean radius of
14 each mode. This formulation limits the aqueous SOA formation in aerosols to only
15 include situations in which the deliquescence relative humidity (DRH) for pure sulfate
16 aerosol (set to 0.8) has been reached. We note that the DRH would decrease in mixed
17 sulfate and SOA particles (Brooks et al., 2002; Smith et al., 2012). Thus, the assumption
18 that aqSOA only forms in the pure sulfate aerosols within the model, and the use of 0.80
19 as the DRH may underestimate the formation of aqSOA to some extent. In addition,
20 water uptake by OA was not treated. There are two reasons for this assumption. First, the
21 reactive uptake parameter ($\gamma=0.0029$) for glyoxal that is used for one of the mechanisms
22 studied here was observed for wet sulfate aerosol only (Liggio et al., 2005). Second, OA
23 is less hygroscopic than sulfate, and the uncertainty associated with neglecting the

1 contribution of OA water is expected to be less than uncertainties caused by the observed
2 range of reactive uptake coefficients and the photochemical reaction rate of glyoxal.
3 Liggio et al. (2005) reported a reactive uptake coefficient for glyoxal that varied from
4 8.0×10^{-4} to 7.3×10^{-3} , and Ervens and Volkamer (2010) found that the derived first-order
5 photochemical reaction rate for glyoxal ranges from 0.8 s^{-1} to 7 s^{-1} depending on the
6 chemical composition of different seed aerosols. Finally, we ignored the formation of
7 aqSOA in the water associated with sea salt aerosol. The terrestrial emissions of isoprene
8 and aromatics are much larger than those from marine sources in the IMPACT model, so
9 the amount of glyoxal/methylglyoxal formed from the oxidation of isoprene and
10 aromatics over oceans is smaller than that over continents. AqSOA formed in the aerosol
11 water associated with sea salt is expected to be small as well.

12 A complete list of aqueous phase reactions and their corresponding rate constants are
13 given in Table S1 and Table S8 in the Supplement. Aqueous reactions for sulfates,
14 nitrates, H_2O_2 , O_3 , OH and related radicals have been taken from Jacob (1986), Pandis
15 and Seinfeld (1989), Lelieveld and Crutzen (1990) and Liu et al. (1997); Aqueous
16 reactions for water-soluble organic compounds are based on recently published box
17 modeling studies (Lim et al., 2005; Herrmann et al., 2005; Ervens and Volkamer, 2010;
18 Lim et al., 2010); Aqueous reactions for iron are drawn from Deguillaume et al. (2010)
19 and the Chemical Aqueous Phase Radical Mechanism (CAPRAM) 2.4 (Ervens et al.,
20 2003).

21 While the chemistry of organic species taking place in cloud droplets is relatively well
22 established in experiments and box modeling studies, the chemistry of organic species
23 occurring in wet particles is only now being developed so that very few models have

1 been extended to include organic reactions (Ervens et al., 2011). Ervens and Volkamer
2 (2010) and Lim et al. (2010) proposed different schemes for SOA formation in aerosol
3 water. Ervens and Volkamer (2010) parameterized the SOA formation using simple first
4 order reaction rate constants to fit photochemical chamber experiments. Basically, gas
5 phase glyoxal is taken into aerosol water based on its Henry's law coefficient and is
6 further hydrated to monohydrate and dihydrate glyoxal using explicit hydration
7 coefficients for the hydration kinetics. The dissolved glyoxal, monohydrate and dihydrate
8 glyoxals can react with dissolved OH radicals to form organic acids, or undergo
9 oligomerization using a parameterized first-order photochemical reaction rate k (unit: s^{-1}).
10 The reactions and kinetic coefficients used in this paper are listed in Table S4 in the
11 Supplement. The reactions in Table S4 extend the Ervens and Volkamer (2010) model for
12 glyoxal to include bulk phase reactions of methylglyoxal by adopting kinetic data from
13 the literature.

14 Lim et al. (2010) describe a second aqueous SOA formation mechanism that used a set of
15 detailed radical-radical reactions based on bulk aqueous phase experiments. Gas-phase
16 glyoxal is partitioned into aerosol water based on its effective Henry's law constant
17 (implicitly accounting for its hydration) and then further reacts with dissolved OH
18 radicals to form radical species by H-atom abstraction, which combine with themselves
19 to form dimers and trimers through so called "radical-radical" reactions (Lim et al.,
20 2010). These "radical-radical" reactions compete with reactions of the radicals with
21 dissolved O_2 to form organic acids. In aerosol-water relevant conditions (i.e., 1-10
22 mole/Liter (M) glyoxal concentrations and $10^{-12} - 10^{-11}$ M dissolved OH radicals), over
23 80% of the products are oligomers. Since no kinetic data for methylglyoxal in-aerosol-

1 water reactions were available in Lim et al. (2010), we assumed that 80% of products
2 from the reaction of dissolved methylglyoxal with OH are oligomers and the rest are
3 oxalic acid, which is consistent with the recent work of Lim et al. (2013).

4 **2.2.2. Surface-limited uptake process**

5 As an alternative to the approaches described above that use a detailed gas-phase and
6 aqueous phase chemical mechanism coupled by gas-particle transfer, a simpler method
7 has also been used by Fu et al. (2008) and Lin et al. (2012) to describe the uptake of a gas
8 and its further reaction inside particles. In this method, the loss of gas phase glyoxal or
9 methylglyoxal on aqueous particles or cloud droplets is parameterized using the
10 following equation:

11
$$\frac{d C_g}{dt} = -\frac{1}{4} \cdot \gamma \cdot A \cdot \langle v \rangle \cdot C_g \quad (2)$$

12 Where A is the total surface area of aqueous sulfate aerosols [m^2/m^3], C_g is the
13 concentration of gas phase glyoxal or methylglyoxal, γ is the reactive uptake coefficient,
14 representing the probability that a molecule impacting the particle surface undergoes
15 reaction. The value of γ used in Fu et al. (2008) and Lin et al. (2012) was assumed to be
16 2.9×10^{-3} for both glyoxal and methylglyoxal uptake on aqueous sulfate and cloud
17 droplets. $\langle v \rangle$ is the mean molecular speed of glyoxal or methylglyoxal in the gas phase
18 given by $(8RT/\pi MW)^{-1/2}$ where MW is the molecule weight of glyoxal or methylglyoxal.

19 **2.3. Case set up**

20 As described above, there are still large uncertainties in simulating aqSOA formation in
21 both cloud water and aerosol water. We thus set up six cases to study the sensitivity of

1 aqSOA formation to different methods representing gas-particle mass transfer and
2 subsequent reactions (i.e., multiphase reaction scheme vs. surface-limited uptake
3 method), to the different chemical schemes in cloud and aerosol water reactions, to the
4 cloud water content, and to the inclusion of iron chemistry in the cloud. The descriptions
5 of these six cases are presented here (also summarized in Table 1), and comparisons of
6 sensitivity test simulations with Case 1 as well as with observations are shown in Sect. 3.

7 In Case 1, we used the detailed multiphase reaction scheme (Eq. 1a, b) to predict the
8 production of glyoxylic acid, oxalic acid and pyruvic acid in both cloud water and aerosol
9 water together with the kinetic uptake of glyoxal and methylglyoxal in both cloud and
10 aerosol water described in Sect. 2.2.1. In addition, in aerosol water we used the surface-
11 limited uptake method (Eq. 2) to predict the formation of oligomers from glyoxal and
12 methylglyoxal. The aqueous phase reactions of organic species used in this case are
13 shown in Table S3 in the Supplement. Reaction rate constants were adopted from Jacob
14 (1986), Pandis and Seinfeld (1989), Lim et al. (2005), Herrmann (2003), and Herrmann et
15 al. (2005). For simplicity, we did not consider the effect of ionic strength of cloud water
16 on the solubility of organics, though this is expected to increase aqSOA formation
17 (Myriokefalitakis et al., 2011). We adopted a reactive uptake coefficient γ of 3.3×10^{-3}
18 from Waxman et al. (2013) to simulate the formation of oligomers due to glyoxal in the
19 aerosol water. The uptake coefficient of methylglyoxal was scaled to that of glyoxal by
20 the ratio of their effective Henry's law constants (Table S7 in the Supplement). This
21 scaling is based on the reasoning that the glyoxal and methylglyoxal uptake by aerosol
22 water correlates with their water solubility and that glyoxal and methylglyoxal have
23 similar chemical reactivity and undergo similar reactions in aerosol water (Lim et al.

1 2013). It might appear that the chemistry for Case 1 double counts the loss rate of
2 glyoxal since it includes both a loss rate by reaction with OH as well as a loss rate due to
3 a surface reaction characterized by an uptake parameter. However, the uptake parameter
4 used in Case 1 was adopted from Waxman et al. (2013), who used a box model to test
5 several chemical mechanisms, in order to fit the observed glyoxal concentrations in
6 Mexico City. The best fit chemical mechanism that they found includes an uptake
7 parameter (gamma) of 3.3×10^{-3} as well as the reaction of OH with glyoxal in dilute water.
8 Therefore we also included the uptake parameter together with the OH chemistry in
9 dilute water.

10 In Case 2, all aqSOA formation was simulated using the multiphase reaction scheme. The
11 chemical reactions in cloud water were the same as those used in cloud in Case 1. The
12 parameterized reactions proposed by Ervens and Volkamer (2010) (Table S4 in the
13 Supplement) were used for the formation of aqSOA in aerosol water replacing the
14 reactions from Table S3 and the uptake coefficients used in Case 1.

15 Case 3 also used the multiphase reaction scheme, but used the bulk reactions adopted
16 from Lim et al. (2010) to predict the formation of aqSOA in both cloud and aerosol
17 water. The detailed bulk phase reactions of organic species used in this case are listed in
18 Table S5 in the Supplement. In this case, we include the further oxidation of oligomers
19 by aqueous phase OH (see the reaction R38, R42, R53, and R54 in Table S5). These
20 further reactions were not included in the Case 1, because the uptake parameter
21 represents the probability that a molecule impacting the aerosol surface will result in
22 uptake and formation of a species which does not evaporate, and this already implicitly

1 takes into account any chemical reactions that include the loss of oligomers inside the
2 aerosol.

3 For Case 4, we employed the same chemical mechanism as in Case 1, but used the cloud
4 field output (in-cloud liquid water content and grid-box cloud fraction) from AM3, the
5 atmospheric component of the coupled general circulation model (CM3) developed at the
6 NOAA Geophysical Fluid Dynamics Laboratory (GFDL) (Donner et al., 2011) in place
7 of the NCAR CCM2 parameterization. Cloud water is a prognostic variable in the GFDL
8 AM3 while it is diagnosed in CCM2.

9 In Case 5, we added iron chemistry in cloud water (Table S6 in the supplementary
10 material) to the chemistry used in Case 1. The only source of aqueous Fe in the model is
11 the dissolution of dust aerosol particles incorporated into cloud droplets. We assumed
12 that 3.5% of the mass of dust aerosol is composed of Fe (Taylor and McLennan, 1985),
13 only 5% of which could be dissolved into cloud water (Ito and Xu, 2014). The initial
14 speciation of Fe(II)/Fe(III) was set to 4 (Deguillaume et al., 2010). This scheme cannot
15 describe the spatial and time variations in dissolved Fe that are predicted in models that
16 include a kinetic description of Fe dissolution (Johnson and Meskhidze 2013, Ito and
17 Feng, 2010) but is able to provide a first-order approximation of the dissolved iron
18 content in cloud water (Table S9 in the Supplement).

19 For Case 6, we used the surface-limited uptake process to simulate all aqSOA formation
20 in both cloud and aerosol water, following the method of Fu et al. (2008) and Lin et al.
21 (2012).

1 **3. Results & Discussion**

2 Table 2 shows the global budget of total aqSOA and each of its components (i.e.,
3 glyoxylic acid, pyruvic acid, oxalic acid and oligomers) (if available) for these six cases.
4 We note that the predicted oligomers in the model can consist of different numbers of
5 monomers (e.g., dimers, trimers and tetramers), so that the total oligomers shown in
6 different cases in Table 2 do not necessarily consist of identical species. We will focus on
7 the detailed budget and global distributions of aqSOA for Case 1 in Sect. 3.1 and Sect.
8 3.2, and the difference between this case and other cases in Sect. 3.3 to Sect. 3.6.

9 **3.1. Global budget**

10 For Case 1, the net global aqSOA production rate totals 20.1 Tg/yr, over 95% of which is
11 removed by wet deposition while the rest is removed by dry deposition. This rate is
12 comparable to the SOA production rate of 28.0 Tg/yr formed from gas-particle
13 partitioning and the rate of 26.0 Tg/yr formed from epoxide predicted in the model. The
14 global annual mean aqSOA burden equals to 0.18 Tg, corresponding to a global mean life
15 time of about 3.0 days due to deposition. Five aqSOA species are predicted: glyoxylic
16 acid, pyruvic acid, oxalic acid, and two classes of oligomers formed from glyoxal and
17 methylglyoxal. Among these five aqueous SOA components, oxalic acid accounts for
18 about 51.7% of the total aqueous SOA source, glyoxal oligomers account for about
19 34.3%, glyoxylic acid for about 11.9%, methylglyoxal oligomers for 1.1% and pyruvic
20 acid for 1.0%. While all oligomers are assumed to be formed in aerosol water, organic
21 acids can be formed in both cloud and aerosol water. However, the contribution of
22 aerosol water to the formation of organic acids formations is very small. The net

1 production rate of glyoxylic acid in the aerosol water accounts for only 0.013 Tg/yr of the
2 total 2.4 Tg/yr net production rate; similarly, only 2.53×10^{-4} Tg/yr of the total 0.17 Tg/yr
3 pyruvic acid is formed in aerosol water; for oxalic acid, the net production rate in the
4 aerosol water (after consumption by reaction with OH) is -0.43 Tg/yr, compared to the
5 total net production rate of 10.4 Tg/yr in cloud water.

6 The global average reaction rates for these organic acids within cloud for case 1 are listed
7 in Table 3. The glyoxylic acid production rate is 15.8 Tg/yr, which is derived from the
8 oxidation of glyoxal, glycolaldehyde, methylglyoxal and acetic acid. Glyoxal oxidation
9 accounts for 77.2%, while the oxidation of glycolaldehyde, methylglyoxal and acetic acid
10 account for 13.9%, 0.7% and 8.2%, respectively. 85.4% of glyoxylic acid is destroyed by
11 reaction with OH and NO_3 , and the rest is deposited to the surface in wet deposition. For
12 oxalic acid, the global production rate in cloud is equal to 15.5 Tg/yr, which is similar to
13 the estimate of 14.5 Tg/yr in Liu et al. (2012) but smaller than the estimate of 21.2 Tg/yr
14 in Simulation S1.1 of Myriokefalitakis et al. (2011), which excluded the effect of the
15 ionic strength of cloud water on glyoxal, glycolaldehyde and methylglyoxal, as we do
16 here. The reaction of glyoxylic acid with OH is a large contributor (94%) to the total
17 oxalic acid production while the reaction with NO_3 contributes the rest. Oxalic acid is
18 removed from the atmosphere through its reaction with OH and NO_3 radicals in the
19 aqueous phase (29.6%) and by wet and dry deposition (71.4%). The chemical destruction
20 rate of oxalic acid is 4.6 Tg/yr. This is smaller than the estimate in Simulation S1.1 of
21 Myriokefalitakis et al. (2011) but larger than that estimated by Liu et al. (2012).
22 Subtracting the chemical destruction rate from the production rate, the global net
23 production rate of oxalic acid is 10.9 Tg/yr, which is slightly smaller than the value of

1 13.2 Tg/yr in Simulation S1.1 of Myriokefalitakis et al. (2011) and the estimate of 13.5
2 Tg/yr in Liu et al. (2012). The only sources of pyruvic acid are the reactions of
3 methylglyoxal with OH and NO_3 . Over half (72.9%) of the pyruvic acid is removed by
4 reactions with OH and NO_3 radicals. For glyoxal and methylglyoxal oligomers, no
5 chemical destruction is included in the model, so these are only removed by wet and dry
6 deposition.

7 The above analysis shows the importance of glyoxal, glycolaldehyde, methylglyoxal and
8 acetic acid as precursors leading to aqueous SOA formation. The global budgets of these
9 four species for Case 1 are summarized in Table 4. While all of glyoxal, glycolaldehyde
10 and methylglyoxal are generated by the oxidation of VOCs in the gas and aqueous phase,
11 around half of the acetic acid is directly emitted into the atmosphere through biomass
12 burning. The global glyoxal production in the gas phase is equal to 69.6 Tg/yr, while
13 reactions in cloud water contribute 3.4 Tg/yr from the oxidation of dissolved
14 glycolaldehyde. About 68.5% of the total glyoxal is consumed in the gas phase, while
15 24.4% is oxidized in cloud and taken up by aqueous aerosol. The rest is deposited to the
16 surface. The total source of methylglyoxal is 167.3 Tg/yr. Of this, only 0.88 Tg/yr and is
17 absorbed and oxidized in cloud and in aqueous aerosol. Most of the methylglyoxal is
18 destroyed in the gas phase or deposited to the surface. The net chemical production of
19 glycolaldehyde in the gas phase is about 17.8 Tg/yr, of which 29.8% is dissolved into
20 cloud and reacts with OH and NO_3 . For acetic acid, the uptake rate by cloud is 0.82
21 Tg/yr, which can be compared to its total source strength of 60.9 Tg/yr. The uptake rate
22 of acetic acid is smaller than the estimate of 6.96 Tg/yr by Liu et al. (2012). This is
23 because of the smaller total atmospheric source strength of acetic acid (60.9 Tg/yr vs. 78

1 Tg/yr), the larger portion of gas-phase consumption of acetic acid (43% vs. 32%), and the
2 smaller Henry's law constant ($3500 \text{ mol L}^{-1} \text{ atm}^{-1}$ vs. $8800 \text{ mol L}^{-1} \text{ atm}^{-1}$) in our model
3 compared to those in Liu et al. (2012). Aqueous aerosol contributes a negligible amount
4 to the sinks of both glycolaldehyde and acetic acid.

5 **3.2. Global distribution and seasonal variability**

6 Figure 1 presents the global annual mean surface mass concentrations (at approximately
7 970 hPa) of total aqSOA, total organic acids (i.e., glyoxylic acid, pyruvic acid and oxalic
8 acid) which are mostly formed in cloud, and oligomers formed in aqueous aerosol. The
9 zonal mean vertical distributions are also shown. The total aqSOA concentrations show
10 large values over tropical Africa, the Amazon basin, Eastern Asia, Eastern United States
11 and Europe. The SOA distributions are determined by their precursor (mainly glyoxal)
12 distributions, oxidant (which is primarily dissolved OH radicals) distributions, and the
13 availability of cloud water or aerosol water. The maximum SOA concentrations over
14 tropical Africa and the Amazon basin reflect the large biogenic VOC emissions and the
15 resulting glyoxal concentration to a great extent. The different patterns shown for organic
16 acid concentrations (Fig. 1C) and for methylglyoxal and glyoxal derived oligomer
17 concentrations (Fig. 1E) are due to the different patterns of cloud and aerosol water
18 content (Fig. 2). Aerosol water content is due to sulfate, which peaks over the industrial
19 regions in the Northern Hemisphere because the largest source of sulfate is from
20 anthropogenic emissions. In contrast, most of the cloud water is located over the tropics
21 and the Southern Hemisphere. This contrast is also reflected in the vertical zonal mean
22 distributions of organic acids and oligomers (Fig. 1D and Fig. 1F). There is a hot spot in
23 organic acids over the tropics, most of which are formed in cloud, while the peak is

1 located over the Northern Hemisphere for the oligomers, all of which are formed in
2 aqueous aerosols.

3 The column burdens of organic acids and oligomers in winter (December, January and
4 February) and in summer (June, July, and August) are presented in Fig. 3. During the
5 winter, the column burden of organic acids peaks over tropical land areas because of the
6 huge biogenic emissions in these regions. During the summer, a secondary column
7 burden maximum arises over the Northern Hemisphere land areas, which can be
8 attributed to the enhanced photochemistry and biogenic emissions over these regions in
9 the summer. The combination of enhanced photochemistry and larger biogenic emissions
10 can increase the production of aqSOA precursors (e.g., glyoxal) and aqueous OH
11 radicals, the latter due to increased H_2O_2 photolysis in cloud. For the same reason, the
12 column burden of oligomers in the summer shows larger values that are spread over a
13 wider area than those in the winter over the Northern Hemisphere (see the right panels in
14 Fig. 3).

15 **3.3. Surface-limited uptake method vs. multiphase reaction scheme**

16 As shown in Table 2, the production rates of oligomers in Case 1 are higher than those in
17 Case 2, which suggests that the value of the reactive uptake coefficient γ adopted from
18 Waxman et al. (2013) is higher than that implied by the simulation with the Ervens and
19 Volkamer (2010) aqueous phase aerosol chemical mechanism. Indeed, we can derive a
20 global averaged γ from the Eq. (2) for the uptake of glyoxal or methlglyoxal into
21 aqueous aerosol from Case 2. We integrated the left side and the right side of Eq. (2)

1 globally and annually, and thus obtained a global averaged annual mean reactive uptake
2 probability from the following equation:

3 $\bar{\gamma} = (\sum \frac{d C_g}{dt}) / (\sum -\frac{1}{4} \cdot A \cdot \langle v \rangle \cdot C_g)$ (3)

4 The derived global averaged $\bar{\gamma}$ for the uptake of glyoxal into the aqueous aerosol is
5 1.41×10^{-5} , while the $\bar{\gamma}$ for the uptake of methylglyoxal into the aqueous aerosol is
6 1.47×10^{-5} . This value for glyoxal uptake is much smaller than the value of 3.30×10^{-3}
7 suggested by Waxman et al. (2013) or the value of 2.90×10^{-3} derived by Liggio et al.
8 (2005). The value derived here for methylglyoxal uptake is comparable to the value of
9 2.92×10^{-5} that we used for methylglyoxal uptake in Case 1. The reason for the
10 discrepancy between measurement studies (i.e. Waxman et al. (2013) and Liggio et al.
11 (2005)) and the values derived here might be that the actual value of the uptake parameter
12 in remote and rural regions is smaller than that derived in urban regions (i.e. Mexico city
13 in the case of Waxman et al. (2013)) or/and that the bulk phase reactions adopted from
14 Ervens and Volkamer (2010) may not include the full set of reactions of glyoxal that are
15 accounted for in the uptake parameter method. In particular, the smaller uptake parameter
16 in rural regions than in urban regions might be due to weaker particle acidity and lower
17 dissolved organic compound concentration in rural regions. The glyoxal uptake rate is
18 observed to be higher in more acidic particles (Liggio et al., 2005). The more
19 concentrated organic compounds in aerosol water might lead to a higher oligomer
20 formation rate (Tan et al., 2009). Also, the bulk phase reactions do not include any
21 surface reactions of glyoxal that the uptake parameter method would include. We note
22 that the derived uptake parameter of order 1×10^{-5} is a globally averaged uptake

1 parameter. Of course, the spatial aqSOA burden which would be predicted using this
2 global average uptake parameter would be different than that predicted using the explicit
3 aqueous formation mechanism. While deriving gamma in lab studies is useful, this
4 method for determining gamma assumes that all of the gas incorporated into the aqueous
5 phase stays in this phase. The explicit chemistry scheme is more demanding of computer
6 time than the use of a single gamma, but it is able to capture the dynamic evolution of
7 aqSOA formation.

8 **3.4. The effect of cloud water content**

9 The global near-surface distribution of grid-box averaged cloud water content for Case 4
10 is shown in Fig. 4(A) while Fig 4(B) shows the zonal annual mean distribution. The
11 cloud water content in Case 1 (Fig. 2) is higher than that in Case 4 almost everywhere
12 below about 900 hPa, leading to larger global organic acids sources and burdens (Table
13 2). The averaged cloud water content and the net SOA production rate in cloud below
14 about 900 hPa in Case 1 is 2.7 times and 4 times higher than those in Case 4,
15 respectively. Figure 4(C) shows the ratio of cloud water content in Case 1 to that in Case
16 4 while Figure 4(D) shows the ratio of the aqSOA production rate in cloud. Both the
17 pattern and value of these ratios are generally similar below about 900 hPa, but above
18 900hPa neither the pattern nor the value is similar. He et al. (2013) studied the
19 relationship between the aqueous SOA formation and cloud water content and proposed a
20 parameterization in which its formation rate is linear in the cloud water content and
21 correlates nonlinearly (concavely) with the total glyoxal and methylglyoxal precursor
22 carbon chemical loss. At lower altitudes where the cloud water concentration in Case 1 is
23 more than a factor of 4 larger than that in Case 4, the linear effect of the change in cloud

1 water content would be expected to dominate the change in the aqSOA production rate.
2 At higher altitudes (approximately between 900 hPa and 200 hPa) where the ratio of
3 cloud water content between in Case 1 and in Case 4 is less than 4, the effect of the
4 change in precursor concentrations (mainly due to the change of wet deposition rates as
5 we show below) may dominate the change in the aqSOA production rate.

6 The lifetime of oxalic acid with respect to deposition in Case 4 is longer than that in Case
7 1 (4.9 days in Case 4 vs. 2.1 days in Case 1), because in Case 4 more oxalic acid is
8 produced at high altitudes or high latitudes and less (by a factor of over 10) is formed at
9 low altitudes in tropical regions (Fig. 4(D)). Oxalic acid can be precipitated out more
10 easily in the tropics than in other regions because precipitation amounts are larger,
11 especially that due to convective precipitation. For similar reasons, we predict a longer
12 lifetime of sulfate aerosol in Case 4 than that in Case 1. In addition, a slightly larger
13 aqueous phase production rate of sulfate aerosol (93.3 Tg/yr) is also found in Case 4
14 compared to that in Case 1 (91.6 Tg/yr). This results from the more abundant cloud water
15 in Case 4 in the Northern hemisphere, where most of sulfate is formed. The longer
16 lifetime and larger aqueous production rate of sulfate causes a larger sulfate burden and
17 thus a larger oligomer formation rate in sulfate aerosol water.

18 **3.5. The effect of iron chemistry in cloud**

19 Inclusion of iron chemistry in cloud decreases the global average net production of
20 oxalate by 57.6%, although it increases both the chemical production and destruction of
21 carboxylic acids in cloud (Table 2). The increase of the chemical production rate is due to
22 the increase of the aqueous OH radical source. Figure 5 depicts the global distribution of

1 annual mean aqueous OH radical concentrations near 971 hPa for Case 1 and Case 5. The
2 largest increase of aqueous OH radicals due to the inclusion of iron chemistry occurs over
3 regions where there are abundant dust aerosols. Arakaki et al. (2013) estimated the
4 steady-state concentrations of OH in cloud sampled over North American remote
5 continental regions. The estimated average OH concentration is 7.2×10^{-15} mol/L. The
6 predicted average OH concentration in this region is 9.0×10^{-14} mol/L in Case 5 and
7 8.8×10^{-14} mol/L in Case 1. Thus the modeled OH concentrations in cloud for both cases
8 are higher than those estimated by Arakaki et al. (2013). Arakaki et al. (2013) also
9 estimated that the averaged total OH production rate in cloud is 1.9×10^{-9} mol/L/s and OH
10 loss rate constant is 2.6×10^5 s⁻¹. In the model, the averaged total OH production rate in
11 this region is 1.06×10^{-8} mol/L/s in Case 5 and 1.03×10^{-8} mol/L/s in Case 1. The OH loss
12 rate is 1.18×10^5 s⁻¹ in Case 5 and 1.17×10^5 s⁻¹ in Case 1. This comparison suggests that
13 the overestimation of OH source is the major reason for the higher OH concentration in
14 the model. Arakaki et al. (2013) attributed the higher OH concentration in cloud water
15 predicted in most box models to their underestimation of OH loss rates. This is not the
16 case in our model. Our OH loss rate of about 1.2×10^5 s⁻¹ compares to values obtained in
17 those box models that range from 2.0×10^4 s⁻¹ to 7.7×10^4 s⁻¹ (Table S2 in Arakaki et al.
18 (2013)).

19 The global aqueous OH radical source in the troposphere (below approximately 200 hPa)
20 in Case 5 is 2.6 times larger than that in Case 1 because of the formation of OH radical
21 through the reaction of Fe(II) with H₂O₂ and the photolysis of Fe(III) oxalate complexes.
22 The largest increase occurs over the Sahara desert, Northwestern China and Mongolia
23 where there are large amounts of dust aerosol (Fig. 5). The enhancement of aqueous OH

1 radicals leads to an increase of 10.8 Tg/yr in the oxalate chemical production rate and
2 partly accounts for an increase of 16.8 Tg/yr in the oxalate chemical destruction rate.
3 Another reason for the increase in the oxalate chemical destruction rate is the fast
4 photolysis of the iron-oxalate complex $[\text{Fe}(\text{C}_2\text{O}_4)_2]^-$, which transforms $\text{C}_2\text{O}_4^{2-}$ to CO_2 .
5 The larger increase in the chemical destruction rate compared to the chemical production
6 rate results in a decrease in the net chemical production rate (6.0 Tg/yr) of oxalate, and
7 thus a decrease in the burden as well. Iron-oxalate complex photolysis accounts for 21.7
8 Tg/yr of oxalate destruction, while the destruction rate through OH and NO_3 reactions is
9 1.20 Tg/yr. This significant sink of oxalate by Fe-complex photolysis is consistent with
10 the finding by Sorooshian et al. (2013) who observed that oxalate concentrations are
11 negatively correlated with observed Fe concentrations. Sorooshian et al. (2013) used a
12 box model to simulate oxalate formation with and without Fe chemistry. They found that
13 the oxalate concentration would decrease when increasing the dissolved iron
14 concentration, but gradually levels off at 15% of the concentration predicted without
15 consideration of Fe chemistry. Our model results show that the oxalate concentration
16 with iron chemistry is about 44% of that predicted without iron. The inclusion of iron
17 chemistry decreases the formation rate of glyoxal oligomers from 6.9 Tg/yr in Case 1 to
18 6.6 Tg/yr in Case 5, which is due to the increased absorption rate of glyoxal in cloud and
19 thus less glyoxal uptake in aqueous aerosol. The absorption rate of glyoxal in cloud is
20 increased because the increased OH radicals in cloud cause more glyoxal to be consumed
21 in cloud so that more gas phase glyoxal can be taken up by cloud.

1 **3.6. SOA formation in clouds vs. SOA formation in aerosol water**

2 On a global average basis, the fraction of SOA formed in cloud varies from case to case,
3 ranging from 44.4% in Case 4 to 103.2% in Case 3 (Table 5). SOA formed in cloud water
4 accounts for about 70% and 80% of total aqSOA in Case 1 and Case 6, respectively; the
5 net SOA production rate in aerosol water is less than zero in Case 2 and Case 3, which
6 means that aqSOA is consumed in aerosol water. This is because the oxalic acid formed
7 in cloud subsequently dissolves into the aerosol water after cloud water evaporates and
8 then further reacts with the high concentration of dissolved OH radicals inside the aerosol
9 water, as shown in Section 3.1. The rate of destruction of oxalic acid by reaction with OH
10 is larger than that of the rate of production from the reaction of glyoxylic acid with OH.
11 Nevertheless, oligomers can still form in the aerosol water, with a production rate of
12 4.5×10^{-2} Tg/yr and 3.6×10^{-2} Tg/yr for Case 2 and Case 3, respectively. The amount of
13 oligomers formed in the aerosol water is similar for Case 2 and Case 3 consistent with the
14 finding by Ervens et al. (2011), who showed that their parameterized reaction system
15 produces a similar amount of SOA as that of Lim et al. (2010) in box model simulations.
16 The relative importance of SOA formed in cloud water decreases to 44.4% in Case 4
17 when using the GFDL AM3 cloud field because of the decrease in the cloud water
18 content in the tropics together with the increased cloud water content in the Northern
19 Hemisphere. In Case 5, which includes iron chemistry in cloud, the SOA production rate
20 in cloud explains 52.9% of total aqSOA production rate (see the Sect. 3.5. for details).

21 **3.7 Discussion of uncertainties**

22 While we have discussed a number of uncertainties concerning the production of aqSOA,

1 there are additional uncertainties that need to be explored. Liu et al. (2012) used a global
2 model to study the sensitivity of their predicted aqSOA in cloud to cloud lifetime, cloud
3 droplet size and cloud fraction. They found that the predicted aqSOA was sensitive to the
4 cloud lifetime and cloud fraction while it depended only weakly on the cloud droplet size.
5 Waxman et al. (2013) studied the sensitivity of aqSOA formation in aerosol to aerosol
6 size distributions. Little size dependence was reported for the case using the multiphase
7 reaction scheme, but the uptake method showed a strong sensitivity to size distribution
8 because of changes in the surface to volume ratio.

9 Furukawa and Takahashi (2011) used X-ray absorption fine structure spectroscopy
10 (XAFS) to show that most of the oxalate within aerosol particles is present as metal
11 oxalate complexes, especially as Ca and Zn oxalate complexes. Xing et al. (2013) also
12 suggest the formation of a stable Zn oxalate complex in the aerosol phase in urban
13 aerosols over China. These complexes are weakly water soluble and very stable, which
14 prevents oxalate from being oxidized by OH in aerosol water. We did not include these
15 effects in our model due to the lack of detailed information, but it is clear that their
16 inclusion could increase the amount of oxalate in aerosol water.

17 Many studies have suggested a 2~3 order of magnitude enhancement in the effective
18 Henry's law constant for glyoxal for aerosol conditions compared to cloud conditions
19 (Kroll et al., 2005; Volkamer et al., 2009; Kampf et al., 2013). To test the potential effect
20 of this enhancement, we added a sensitivity test based on Case 3 but increased the
21 effective Henry's law constants of glyoxal and methylglyoxal for aerosol water by 3
22 orders of magnitude. In this sensitivity case, the chemical production rate of glyoxal
23 oligomer is 4.65×10^{-1} Tg/yr, and the chemical destruction rate is 1.95×10^{-1} Tg/yr,

1 leading to a net production rate that is roughly a factor of 10 larger than that in Case 3,
2 1.95×10^{-1} Tg/yr. The net production rate for methylglyoxal oligomer is increased by more
3 than a factor of 10, to 8.68×10^{-2} Tg/yr. These increases in net production rates lead to an
4 increase in oligomer burden by a factor of 4.4. However, these enhanced net production
5 rates and global burdens are still smaller than those predicted in the Case 1 which adds
6 the Waxman et al. (2013) uptake method for the production of aqSOA in aqueous
7 aerosol.

8 The formation and loss of oxalate by aqueous phase OH depends strongly on the pH
9 value (see reactions R2-6 in Table S3), because the rate constants of oxidations of
10 glyoxylic acid and oxalic acid are smaller than those of their anions (i.e., glyoxylate and
11 oxalate) and the relative abundance of these acids and their anions depends on pH values.
12 We present the predicted annual mean pH in cloud near 971 hPa in Figure S1 in the
13 Supplement and compare our predicted pH values with observations from the literature
14 (Table S10 in the Supplement). The results agree with predictions at some locations, but
15 show that the model is too acidic in other locations. We would expect the oxalate
16 concentrations to vary little if pH values were increased, because both the formation rate
17 and the destruction rate of oxalate would increase. This weak dependence of aqSOA
18 formed in cloud has been observed in a parcel model that included a multiphase reaction
19 mechanism similar to that which we use in this work (Ervens et al., 2008).

20 The comparison of Case 2 and Case 3 with Case 1 shows that the use of only the
21 multiphase reaction scheme for aerosol water decreases the global total aqSOA burden by
22 around 50%. In the case which increases the effective Henry's law constant by 3 orders
23 magnitude, the aqSOA burden remains lower than that predicted in Case 1 by 42%. The

1 replacement of diagnostic cloud field with GFDL AM3 cloud field causes the burden to
2 increase by 16%. In the case including iron chemistry in cloud, the burden is predicted to
3 be smaller than that in Case 1 by 11%. The use of the uptake parameter method for both
4 cloud water and aerosol water in Case 6 predicts a 185% larger burden than Case 1.

5 **4. Comparison with measurements**

6 In this section, we compare model results to measured oxalate, AMS measurements of
7 SOA, and SOA O/C ratios. Oxalate is a major component of aqSOA formed in cloud, and
8 thus the comparison of oxalate with observations gives us a direct evaluation of the
9 modeled aqSOA, while comparison of SOA measured by AMS data and O/C ratios can
10 indirectly constrain the modeled aqSOA.

11 **4.1. Oxalate**

12 Figure 6 compares the modeled oxalic acid near 971 hPa with the measured oxalate
13 compiled in Table S3 of Myriokefalitakis et al. (2011). We only show this comparison for
14 Case 1, Case 4, and Case 5, since the oxalic acid concentrations in the other cases are
15 similar to those in Case 1 (Table 2). Although oxalate measurements are sparse around
16 the world, the observations listed here cover values over most continents: United States,
17 Europe, China, Amazon basin and Africa. These measurements have time sampling
18 durations which span from several days up to 2 years. For this comparison, the monthly
19 simulation data were sampled for the specific month and at the specific location
20 corresponding to the measurements. It should be noted that due to the coarse resolution
21 used in the model (4 degrees by 5 degrees), we do not expect the model to be able to
22 predict the high concentrations seen in urban regions and hence we leave these out. Over

1 rural areas, the model performance varies in different regions and different seasons. In
2 Europe, the results for Case 1 underestimate almost all observations, although the results
3 for summer are relatively better (green triangles in Fig. 6) than those in winter (black dots
4 in Fig.6). The difference in the model performance between in summer and in winter may
5 be attributed to different oxalate sources in these two seasons. According to Legrand et
6 al. (2007), the major oxalate sources at the CARBOSOL surface stations in winter are
7 fast secondary production in wood burning plumes and secondary production through the
8 rapid oxidation of toluene and ethane emitted from vehicles. In summer these
9 anthropogenic emissions decrease and biogenic emissions (e.g., isoprene) increase and
10 make an important contribution to the oxalate source via multiphase photochemical
11 reactions. These four CARBOSOL sites are included in the comparison here and we
12 suspect the other European sites that we included have similar oxalate sources to those at
13 the CARBOSOL sites. Unlike what is expected for the measurements, the model can not
14 represent the rapid secondary formation of oxalic acid from local sources. Other factors
15 which might also contribute to the model under-estimation include a low cloud water
16 content or high deposition rates in the model. When using the GFDL AM3 cloud field,
17 the model prediction improves at some sites.

18 As shown by the red squares in Fig. 6, the model also significantly underestimates the
19 measured oxalate concentrations at 2 of the 3 sites in the Amazon basin. One possible
20 reason for this underestimation is that the model does not include the oxalate source from
21 biomass burning either through direct emission or through secondary formation from
22 carbohydrate species in smoke aerosols (e.g., levoglucosan) during aerosol aging (Gao et
23 al., 2003). At these two sites, biomass burning is the major source of oxalate formation

1 (Falkovich et al., 2005; Kundu et al., 2010; Granham et al., 2002). At the site where the
2 aerosol samples were believed to be out of the influence of biomass burning (Talbot et al.
3 1988), the modeled oxalate concentration in Case 1 is higher than the observation, but in
4 Case 4 (using the GFDL AM3 cloud field) the model still underestimates the observation.

5 There are only two sites in China and three sites in US with oxalate measurements for
6 comparison to the model. The model underestimates the observations in China, especially
7 at the Mangshan site, 40 km north of Beijing, polluted by air mass transported from
8 Beijing (He and Kawamura, 2010). This site has a high oxalate concentration of 760
9 ng/m³. The model can't represent the local emissions and thus only captures less than
10 10% of the observation. Using the GFDL AM3 cloud field doesn't improve the model
11 performance. Overestimation of oxalate deposition in the model may also contribute to
12 this under-prediction. The three blue circles in Fig. 6 show the comparisons for the sites
13 in United States, and indicate that the model does reasonably well, except for the site in
14 Sydney, Florida, at which the model still under-predicts the oxalate source or/and
15 overestimates its sink. For the two sites in Africa (red stars in Fig. 6), the model fails to
16 predict the observations. The modeled oxalate concentration in Case 1 is 3 times higher
17 than the observation at the Central Africa site and is only about 1/5 of measured
18 concentration at the South Africa site. This might suggest that the cloud water content in
19 this simulation is inconsistent with the real cloud water content or that the model does not
20 represent the sources and/or sinks of oxalate over this region very well. In Case 4, the
21 model under-predicts the measurements at both of these two sites.

22 When including the iron chemistry in cloud in Case 5, almost all of the modeled oxalate
23 concentrations are lower than the measurements by over a factor of 2. As noted above,

1 this underestimation may be caused by an overestimation of the photolytic rate of the
2 iron-oxalate complex and/or an underestimation of oxalate production rate.

3 The global oxalate burden in case S1 reported by Myriokefalitakis et al. (2011) predicted
4 is 5 times larger than the burden reported here for Case 1. This is partly because
5 Myriokefalitakis et al. (2011) increased the solubility of glyoxal and methylglyoxal in
6 cloud water by 2 orders of magnitude, which is at the high end of measured values,
7 causing a larger oxalate source. Myriokefalitakis et al. (2011) also included a set of
8 additional reactions proposed by Carlton et al. (2007) which were based on experiments
9 that were performed under higher glyoxal concentration conditions than those present in
10 real cloud water. These additional reactions result in more oxalate formation.
11 Myriokefalitakis et al. (2011) lumped these additional reactions to a single reaction (see
12 R21 in Table 1 in Myriokefalitakis et al. (2011)). We note that the reaction rate constant
13 of $3.1 \times 10^9 \text{ L mol}^{-1} \text{ s}^{-1}$ for that lumped reaction was a typo (M. Kanakidou, personal
14 communication, 2014). The reaction rate constant should be $3.1 \times 10^{10} \text{ L mol}^{-1} \text{ s}^{-1}$. In
15 addition, a longer oxalate lifetime with respect to deposition was predicted by these
16 authors. The larger oxalate burden in Myriokefalitakis et al. (2011) leads to a closer
17 agreement with measurements over rural sites. However, the simulations in
18 Myriokefalitakis et al. (2011) did not include iron chemistry in cloud which, as we have
19 shown, can decrease oxalate concentrations significantly (compare Case 1 and Case 5).

20 Figure 6 also shows a comparison of oxalate with observations at marine sites. Most of
21 the modeled oxalate is lower than the measurements. Myriokefalitakis et al. (2011)
22 considered an extra glyoxal source of 20 Tg/yr over the oceans to explain the gap
23 between the glyoxal measured from satellite and that predicted in their model. The

1 underestimation of oxalate at marine sites in our model would also be improved by
2 adding an extra marine source of glyoxal, although the origin of glyoxal in the marine
3 boundary layer is still matter of debate (Rinaldi et al., 2011). As shown above and in
4 Sec. 3.4, cloud water has an important effect on oxalate formation. Therefore it is also
5 valuable to compare the cloud water content in the model with that in measurements.
6 However, there are only a few sites where measured oxalate concentrations were reported
7 together with cloud water content (e.g., Sorooshian et al., 2006; Wonaschuetz et al.,
8 2012). Thus, this comparison is unlikely to be able to discern which source might explain
9 the underestimate.

10 **4.2. AMS measurements**

11 Although there are no measurements available that can separate aqSOA from the SOA
12 formed in the gas phase, we can compare the modeled total SOA with the observed total
13 SOA. The predicted ratio of the global average aqSOA concentration to total SOA
14 concentration ranges from 9.5% in Case 2 to 33.5% in Case 6. Zhang et al. (2007) present
15 observational SOA data (measured by aerosol mass spectrometry, AMS) from a series of
16 surface measurements at multiple sites in the Northern Hemisphere, which were made in
17 different seasons and different years between 2000 and 2006 and were reported for the
18 average of varying durations spanning from 8 to 36 days. Here, we compare the model
19 data at the corresponding grid in the corresponding month. Fig. 7 shows the comparisons
20 of SOA between observations and predictions in Case 1, Case 2, Case 4, Case 5 and Case
21 6. The normalized mean bias (NMB) and correlation coefficient (R) for these
22 comparisons are listed in Table 6. We do not show the comparisons for Case 3 in Fig. 7
23 because the SOA concentrations for this case are close to those for Case 2 (Table 2).

1 Again, we do not expect the model with its low horizontal resolution to capture the POA
2 emissions at urban sites, nor would we capture high local VOC and NO_x emissions,
3 which have a very complex effect on SOA formation due to non-linear chemistry (Stroud
4 et al., 2011). The NMB in Case 1 is -32.4% for rural sites (see the Table 6). The
5 multiphase reactions scheme used for aqSOA in aerosol water in Case 2 leads to a larger
6 underestimation (a NMB of around -42.5%); Using the GFDL AM3 cloud fields allows
7 the model predictions to more closely match the measurements; The model in Case 6,
8 which adopts the reactive uptake method for both aerosols and clouds, overestimates the
9 observations by around 20%.

10 In addition to the AMS measurements made in the Northern Hemisphere extra-tropics
11 reported in Zhang et al. (2007), we also show the comparison with measurements from
12 three different campaigns in tropical forested areas (Table 7). As SOA dominated the
13 total submicron OA in Amazon basin (Chen et al., 2009) and in Malaysian Borneo
14 (Robinson et al., 2011), the comparison of OA in these two sites reflects the model
15 performance of SOA to a large extent. Comparing with the measurements at West Africa
16 reported by Capes et al. (2009), the model predicts both a higher SOA concentration and
17 a higher NO_x concentration. The NO_x concentration has been shown to have a large effect
18 on SOA formation (e.g., Ng et al., 2007), thus, we expect that improving the NO_x
19 predictions might lead to a better SOA simulation. There are two measurements available
20 in Amazon region. Gilardoni et al. (2011) reported average PM_{2.5} organic aerosol
21 concentrations during the wet season (February-June) of 1.7 $\mu\text{g}/\text{m}^3$, larger than the wet
22 season concentrations measured at the same site by Chen et al. (2009) by about 60-80%.
23 In comparison with the measurements reported by Gilardoni et al. (2011), our simulated

1 concentrations in Case 1 to Case 5 are around 60% too high. At the Malaysian Borneo
2 site, the model simulations of SOA are higher than the observation by less than 40% for
3 Case 1 to Case 5. The simulation in Case 6 overestimates the measurements by a factor of
4 3.8 at the West Africa site and by a factor of over 2 at the Amazon and the Malaysian
5 Borneo site.

6 It should be noted that that good agreement between observations and model predictions
7 does not imply a robust understanding of underlying processes. However, the relative
8 trends in how these comparisons change between different cases (Table 8) helps one to
9 understand the benefits of different underlying processes and to determine the best
10 current approach. For the Northern Hemisphere, the uptake method (Case 1 and Case 6)
11 provides an approach that agrees better with the observations while the use of the GFDL
12 cloud field also improves the model performance. In the tropics the use of the multiphase
13 reaction scheme helps to close the gap between the simulation and the observations, and
14 including iron chemistry also decreases the model bias. On the other hand, including iron
15 chemistry degrades the model's ability to predict the oxalate concentrations. Thus there is
16 no single approach that is able to capture all the observations well. Further mechanism
17 development and/or aerosol transport model and general circulation model development
18 of cloud fields are needed to improve the agreement with observations. For example, the
19 inclusion of stable Ca and Zn oxalate complex formation would increase both oxalate and
20 SOA concentrations and thus help to close the gap between the simulation and the
21 observations, as we noted above in Sect. 3.7.

22 **4.3. O/C ratios**

1 It is useful to compare the O/C ratio of our modeled OA to observations, since the O/C
2 ratio in aqueous formation mechanisms is expected to be larger than that in gas phase
3 formation mechanisms. Aiken et al. (2008) derived a significant correlation between the
4 O/C ratios of OA and their f44 signal (the ratio of m/z 44 to the total signal in the mass
5 spectrum) and Ng et al. (2010) used this correlation to estimate the O/C ratio of
6 oxygenated OA (OOA) obtained from a factor analysis of the Northern Hemisphere AMS
7 dataset. Here, we compare the O/C ratios estimated in the model with those reported by
8 Ng et al. (2010) (Fig. 8).

9 In the model, we have four different SOA components: SOA from the gas-particle
10 partitioning of semi-volatile organic compounds (SVOCs), SOA from aerosol phase
11 reactions of these condensed SVOCs, SOA from the uptake of epoxide on sulfate aerosol,
12 and SOA formed in the aqueous phase as described above (aqSOA). We used the
13 following methods to estimate the predicted O/C ratio of these SOA components:

14 (1). For the SOA from the gas-particle partitioning of SVOCs, there are 26 explicit
15 SVOCs that contribute to the SOA formed from gas-particle partitioning. We calculated
16 the O/C ratio for each species based on their chemical formulas (See Table S1 in Lin et al.
17 2012).

18 (2). For the SOA from aerosol phase reactions of condensed SVOCs, however, it is not as
19 straightforward to calculate O/C ratio. First, the aerosol phase reactions of condensed
20 SVOCs were simply treated in the model as first-order reactions to form oligomers with
21 an assumed time constant (nominally 1 day), without any information on the products
22 from these aerosol phase reactions. However, Chen et al. (2011) and Liu et al. (2012)

1 suggested specific aerosol phase reactions for organic hydroperoxides and organic nitrate,
2 respectively, both of which are major components of SVOCs in the model (Lin et al.,
3 2012). Chen et al. (2011) proposed a set of new aerosol phase reactions for organic
4 hydroperoxides: decomposition, followed by radical-radical oligomerization to explain
5 the smaller measured O/C ratios than those predicted in their model. This aerosol phase
6 reaction was shown to remove 1~2 O atoms from organic hydroperoxides. Organic
7 nitrate is thought to undergo hydrolysis in the particle phase (Liu et al., 2012), which
8 removes two O atoms from organic nitrate. Despite the simple treatment for oligomer
9 formation in the model, we assume that the oligomers from organic hydroperoxides and
10 organic nitrate have 1.5 O atoms and two O atoms less than condensed organic
11 hydroperoxides and organic nitrate have, respectively, based on Chen et al. (2011) and
12 Liu et al. (2012). For the oligomers formed from other condensed SVOCs, we assume
13 they have the same O/C ratio as their corresponding SVOCs. An additional complexity is
14 that in the model the 26 SOA species formed from the oligomerization of condensed
15 SVOCs are lumped together as one species when they are transported in the atmosphere.
16 Therefore, we used their global-averaged SOA formation rates (listed in Table S1 in Lin
17 et al. 2012) rather than their mass concentrations to weight their relative contributions to
18 the O/C ratio. Based on these assumptions, we estimate the average O/C ratio for the
19 SOA from aerosol phase reactions of condensed SVOCs to be around 0.687, with values
20 for some of the SVOCs with smaller burdens ranging from 3.0 to 0.3.

21 (3). For SOA from the uptake of epoxide, the O/C ratio is estimated to be 0.6 since the
22 O/C ratio of epoxide from isoprene oxidation is 0.6 in the model, and its oligomerization
23 would not be expected to change the O/C ratio (Surratt et al., 2010).

1 (4). The O/C ratio for oxalic acid is 2, for glyoxylic acid is 1.5, and for pyruvic acid is 1.0.
2 The O/C ratio for oligomers from glyoxal and methylglyoxal is assumed to be 1.5, which
3 is consistent with the measurements by Lim et al. (2010).

4 We then averaged the O/C ratios of these four SOA components by weighting their mass
5 concentrations to obtain the average O/C ratio for total SOA. As shown in Fig. 8, the
6 modeled O/C ratios are higher than those reported by Ng et al. (2010) and have a
7 normalized mean bias of 33%. The higher O/C ratios estimated in the model might
8 suggest an overestimation of the contribution of aqueous SOA formation or multiple
9 generation oxidation products to SOA formation or a missing aerosol phase reaction of
10 condensed SVOCs that would lead to products with lower O/C ratios. Alternatively, the
11 AMS instrument might underestimate O/C ratios.

12 **5. Conclusions**

13 In this paper, we simulated the formation of SOA in both cloud and aerosol water using
14 multiphase processes with different chemical reactions as well as a surface-limited uptake
15 process. We also conducted a simulation using the GFDL AM3 cloud fields and a
16 simulation including iron chemistry in cloud.

17 The annual average organic acid concentration (i.e. the sum of oxalic acid, glyoxylic
18 acid, and pyruvic acid) peak over the tropical regions due to the large biogenic emissions
19 and abundant cloud water there, while oligomers generally show a maxima over
20 industrialized areas in the Northern Hemisphere due to formation within aqueous aerosols
21 and the large sulfate aerosol concentrations located in these regions. During the summer,
22 large organic acid concentrations are also predicted in the Northern Hemisphere resulting

1 from seasonally enhanced biogenic emissions and photochemistry. Similarly, the
2 oligomer concentrations increase in the summer.

3 Using the surface-limited uptake process scheme with the reactive uptake parameter
4 adopted from the laboratory studies (Case 6) leads to higher aqSOA production rates both
5 in cloud and in aerosol water than the use of only the multiphase process scheme does
6 (Cases 2 and 3). The use of a multiphase reaction scheme for aerosol water decreases the
7 global total aqSOA burden by around 50% (compare Case 1 and Case 2). The use of the
8 uptake parameter method for both cloud water and aerosol water in Case 6 predicts a
9 185% larger burden than Case 1. An increase of 3 orders magnitude for the effective
10 Henry's law constants of glyoxal and methylglyoxal in aerosol water leads to an increase
11 of 1 order magnitude in oligomer net production rate and an increase in aqSOA burden
12 by 8%. When we changed the diagnostic cloud field to that simulated by the GFDL AM3
13 model, the organic acid production rate decreased by around 60% while sulfate formation
14 rates increased slightly, because the GFDL AM3 cloud field has a much smaller cloud
15 water content in tropical regions but a higher cloud water content in the Northern
16 Hemisphere. The replacement of diagnostic cloud field with GFDL AM3 cloud field
17 causes the aqSOA burden to increase by 16%. The aqSOA formation rate in cloud water
18 is slightly less than in aerosol water in the simulation with the GFDL AM3 cloud field,
19 while in the other simulations with the diagnostic cloud field the aqSOA formation rate in
20 cloud water dominates over that in aerosol water. The introduction of Fe chemistry in
21 cloud has a large impact on the aqueous phase OH and aqSOA budget, increasing the
22 global average tropical aqueous OH radical source by a factor of about 2.6 and
23 decreasing the net source and burden of aqSOA by 31% and 11%, respectively.

1 We also compared the oxalic acid predicted from these different schemes and chemical
2 mechanisms with measurements obtained in Europe, Amazon, Africa, China and US
3 region. Overall, the model tends to underestimate observations, probably because it does
4 not account for the direct emission of oxalic acid from primary sources (e.g., wood
5 burning, meat cooking and biomass burning) or the oxalic acid formed in the aging
6 process associated with emissions plumes. However, this underestimation might also be
7 due to a deposition rate that is too high or to a cloud water content that is too low in the
8 model. In fact, using the GFDL AM3 cloud field in Case 4 improved the model
9 predictions at some sites in the Northern Hemisphere. Consistent with the findings of
10 Myriokefalitakis et al. (2011) and Rinaldi et al. (2011), the comparison of oxalate for
11 marine sites suggests that there may be a missing source of oxalic acid over the ocean.
12 When including the iron chemistry in cloud, the model under-predicts all of the measured
13 concentrations of oxalate by over a factor of 2.

14 Comparisons of the total SOA (aqSOA combined with the SOA formed in the gas phase)
15 for all cases with the SOA measured by AMS in the Northern Hemisphere show
16 reasonable agreement, although the NMB varies between +20% in Case 6 (which used a
17 surface-based uptake coefficient method for aqSOA both in cloud and aerosol water) to
18 around -42% in Cases 2 and 3 (which used a complete or a parameterized multiphase
19 reaction scheme for aqSOA). While Case 6 over-estimates the observations by a factor
20 of over 3 at a West Africa site and by over a factor of 2 at the two other tropical sites,
21 adopting the multiphase reaction scheme for aqSOA decreases the disagreement to within
22 a factor of 2 at all three sites. In addition to the SOA mass measured by AMS, we
23 compared the O/C ratio of OOA estimated based on a factor analysis of AMS

1 measurements to the O/C ratio of modeled SOA based on some simple assumptions. The
2 estimated O/C ratios from the model are somewhat higher than those estimated from the
3 measurements, which might indicate that the model somewhat overestimates the
4 contribution of aged organic species and/or aqueous SOA formation to the total SOA
5 formation.

6 In our study, we were unable to find a single mechanism that is able to capture all
7 observations well. The cases that use an uptake coefficient method for aerosol water
8 perform better than the cases using the multiphase reaction scheme in comparison to the
9 Northern Hemisphere AMS measurements. However, in the tropics, the use of a
10 multiphase process scheme for both aerosol water and cloud water perform best, while
11 the case using the uptake coefficient method in cloud water clearly overestimates the
12 observed OA by more than a factor 3. The multiphase reaction scheme including iron
13 chemistry under predicts the observed oxalate concentrations at all sites. Since the
14 inclusion of the formation of stable metal-oxalate complexes in the model is expected to
15 enhance both oxalate and aqSOA concentrations, a multiphase reaction scheme that
16 included this complex formation might work best.

17 Future work is needed to close the gap between simulations and observations. In
18 particular, more lab and model studies are needed to improve the representation of
19 chemical reactions within the aqueous phase and at the gas/aerosol interface, since there
20 is still a large inconsistency between the existing uptake parameter method and the
21 multiphase reaction schemes derived from lab studies and field measurements. Also,
22 more work is needed to improve our understanding of oxalate sources and sinks,
23 especially the formation of stable metal-oxalate complexes, because the model tended to

1 underestimate observed oxalate concentrations for all cases studied. In addition, the high
2 sensitivity of aqSOA to cloud water content shows the importance of improving the
3 representation of cloud water content in general circulation models in order to improve
4 aqSOA formation.

5 **Acknowledgments**

6 The authors are grateful for support by the Department of Energy (DOE) Earth System
7 Modeling program through grant number DOE FG02 01 ER63248, support from the
8 DOE Atmospheric Science Research Program through grant number DoE DE-
9 SC0008486, and support from EPA Science to Achieve Results (STAR) program, grant
10 #R-83337701. A. Ito's work at JAMSTEC was supported under Program for Risk
11 Information on Climate Change by MEXT. The authors thank B. J. Turpin for her helpful
12 suggestions on improving the manuscript as well as the two anonymous reviewers.

13 **References**

14 Aiken, A. C., DeCarlo, P. F., Kroll, J. H., Worsnop, D. R., Huffman, J. A., Docherty, K.
15 S., Ulbrich, I. M., Mohr, C., Kimmel, J. R., Sueper, D., Sun, Y., Zhang, Q., Trimborn,
16 A., Northway, M., Ziemann, P. J., Canagaratna, M. R., Onasch, T. B., Alfarra, M. R.,
17 Prevot, A. S. H., Dommen, J., Duplissy, J., Metzger, A., Baltensperger, U., and
18 Jimenez, J. L.: O/C and OM/OC Ratios of Primary, Secondary, and Ambient Organic
19 Aerosols with High-Resolution Time-of-Flight Aerosol Mass Spectrometry, *Environ.*
20 *Sci. Technol.*, 42, 4478–4485, doi:10.1021/es703009q, 2008.

21 Altieri, K. E., Seitzinger, S. P., Carlton, A. G., Turpin, B. J., Klein, G. C., and Marshall,
22 A. G.: Oligomers formed through in-cloud methylglyoxal reactions: Chemical
23 composition, properties, and mechanisms investigated by ultra-high resolution FT-ICR
24 mass spectrometry, *Atmos. Environ.*, 42, 1476–1490,
25 doi:10.1016/j.atmosenv.2007.11.015, 2008.

26 Altieri, K. E., Turpin, B. J. and Seitzinger, S. P.: Composition of Dissolved Organic
27 Nitrogen in Continental Precipitation Investigated by Ultra-High Resolution FT-ICR
28 Mass Spectrometry, *Environ. Sci. Technol.*, 43(18), 6950–6955,
29 doi:10.1021/es9007849, 2009.

1 Arakaki, T., Anastasio, C., Kuroki, Y., Nakajima, H., Okada, K., Kotani, Y., Handa, D.,
2 Azechi, S., Kimura, T., Tsuhako, A., and Miyagi, Y.: A General Scavenging Rate
3 Constant for Reaction of Hydroxyl Radical with Organic Carbon in Atmospheric
4 Waters, *Environ. Sci. Technol.*, 10.1021/es401927b, 2013.

5

6 Barth, M. C., Sillman, S., Hudman, R., Jacobson, M. Z., Kim, C. H., Monod, A., and
7 Liang, J.: Summary of the cloud chemistry modeling intercomparison: photochemical
8 box model simulation, *J. Geophys. Res.-Atmos.*, 108, 4214,
9 doi:10.1029/2002JD002673, 2003.

10 Blando, J. D. and Turpin, B. J.: Secondary organic aerosol formation in cloud and fog
11 droplets: a literature evaluation of plausibility, *Atmos. Environ.*, 34(10), 1623–1632,
12 2000.

13 Brooks, S. D., Wise, M. E., Cushing, M., and Tolbert, M. A.: Deliquescence behavior of
14 organic/ammonium sulfate aerosol, *J. Geophys. Res.*, 29(19), 1917,
15 doi:10.1029/2002GL014733, 2002.

16 Capes, G., Murphy, J. G., Reeves, C. E., McQuaid, J. B., Hamilton, J. F., Hopkins, J. R.,
17 Crosier, J., Williams, P. I., and Coe, H.: Secondary organic aerosol from biogenic
18 VOCs over West Africa during AMMA, *Atmos. Chem. Phys.*, 9, 3841–3850,
19 doi:10.5194/acp-9-3841-2009, 2009.

20 Carlton, A. G., Turpin, B. J., Lim, H. J., Altieri, K. E., and Seitzinger, S.: Link between
21 isoprene and secondary organic aerosol (SOA): Pyruvic acid oxidation yields low
22 volatility organic acids in clouds, *Geophys. Res. Lett.*, 33, L06822,
23 doi:10.1029/2005GL025374, 2006.

24 Carlton, A. G., Turpin, B. J., Altieri, K. E., Seitzinger, S., Reff, A., Lim, H. J. and
25 Ervens, B.: Atmospheric oxalic acid and SOA production from glyoxal: Results of
26 aqueous photooxidation experiments, *Atmos. Environ.*, 41(35), 7588–7602,
27 doi:10.1016/j.atmosenv.2007.05.035, 2007.

28 Carlton, A. G., Turpin, B. J., Altieri, K. E., Seitzinger, S. P., Mathur, R., Roselle, S. J.,
29 and Weber, R. J.: CMAQ model performance enhanced when in-cloud secondary
30 organic aerosol is included: Comparisons of organic carbon predictions with
31 measurements, *Environ. Sci. Technol.*, 42, 8789–8802, 2008.

32 Chen, J., Griffin, R. J., Grini, A. and Tulet, P.: Modeling secondary organic aerosol
33 formation through cloud processing of organic compounds, *Atmos. Chem. Phys.*,
34 7(20), 5343–5355, doi:10.5194/acp-7-5343-2007, 2007.

35 Chen, Q., Farmer, D. K., Schneider, J., Zorn, S. R., Heald, C. L., Karl, T. G., Guenther,
36 A., Allan, J. D., Robinson, N., Coe, H., Kimmel, J. R., Pauliquevis, T., Borrmann, S.,
37 Pöschl, U., Andreae, M. O., Artaxo, P., Jimenez, J. L., and Martin, S. T.: Mass
38 spectral characterization of submicron biogenic organic particles in the Amazon Basin,
39 *Geophys. Res. Lett.*, 36, L20806, doi:10.1029/2009gl039880, 2009.

40 Chen, Q., Liu, Y., Donahue, N. M., Shilling, J. E. and Martin, S. T.: Particle-Phase

1 Chemistry of Secondary Organic Material: Modeled Compared to Measured O:C and
2 H:C Elemental Ratios Provide Constraints, *Environ. Sci. Technol.*, 45(11), 4763–
3 4770, doi:10.1021/es104398s, 2011.

4 Coy, L. and Swinbank, R.: Characteristics of stratospheric winds and temperatures
5 produced by data assimilation, *J. Geophys. Res.*, 102(D22), 25763–25781, 1997.

6 Coy, L., Nash, E. R. and Newman, P. A.: Meteorology of the polar vortex: Spring 1997,
7 *Geophys. Res. Lett.*, 24(22), 2693–2696, 1997.

8 DeGouw, J. A., Middlebrook, A. M., Warneke, C., Goldan, P. D., Kuster, W. C., Roberts,
9 J. M., Fehsenfeld, F. C., Worsnop, D. R., Canagaratna, M. R., Pszenny, A. A. P.,
10 Keene, W. C., Marchewka, M., Bertram, S. B., and Bates, T. S.: Budget of organic
11 carbon in a polluted atmosphere: Results from the New England Air Quality Study in
12 2002, *J. Geophys. Res.*, 110, D16305, doi:10.1029/2004JD005623, 2005.

14 Deguillaume, L., Desboeufs, K. V., Leriche, M., Long, Y., & Chaumerliac, N.: Effect of
15 iron dissolution on cloud chemistry: from laboratory measurements to model results,
16 *Atmos. Pollut. Res.*, 1(4), 220-228, 2010.

17 Deguillaume, L., Leriche, M. and Desboeufs, K.: Transition metals in atmospheric liquid
18 phases: Sources, reactivity, and sensitive parameters, *Chemical Reviews-Columbus*,
19 105, 3388-3431, 2005.

20 Donner, L. J., Wyman, B. L., Hemler, R. S., Horowitz, L. W., Ming, Y., Zhao, M., Golaz,
21 J.-C., Ginoux, P., Lin, S. J., Schwarzkopf, D. M., Austin, J., Alaka, G., Cooke, W. F.,
22 Delworth, T. L., Freidenreich, S. M., Gordon, C. T., Griffies, S. M., Held, I. M.,
23 Hurlin, W. J., Klein, S. A., Knutson, T. R., Langenhorst, A. R., Lee, H.-C., Lin, Y.,
24 Magi, B. I., Malyshev, S. L., Milly, P. C. D., Naik, V., Nath, M. J., Pincus, R.,
25 Poshay, J. J., Ramaswamy, V., Seman, C. J., Shevliakova, E., Sirutis, J. J., Stern, W.
26 F., Stouffer, R. J., Wilson, R. J., Winton, M., Wittenberg, A. T., and Zeng, F.: The
27 Dynamical Core, Physical Parameterizations, and Basic Simulation Characteristics of
28 the Atmospheric Component AM3 of the GFDL Global Coupled Model CM3, *J.
29 Climate*, 24, 3484–3519, doi:10.1175/2011JCLI3955.1, 2011.

30 Dzepina, K., Volkamer, R. M., Madronich, S., Tulet, P., Ulbrich, I. M., Zhang, Q.,
31 Cappa, C. D., Ziemann, P. J. and Jimenez, J. L.: Evaluation of recently-proposed
32 secondary organic aerosol models for a case study in Mexico City, *Atmos. Chem.
33 Phys.*, 9(15), 5681–5709, 2009.

34 El Haddad, I., Yao Liu, Nieto-Gligorovski, L., Michaud, V., Temime-Roussel, B., Quivet,
35 E., Marchand, N., Sellegrí, K., and Monod, A.: In-cloud processes of methacrolein
36 under simulated conditions – Part 2: Formation of secondary organic aerosol, *Atmos.
37 Chem. Phys.*, 9, 5107–5117, doi:10.5194/acp-9-5107-2009, 2009.

38 Eliason, T. L., Aloisio, S., Donaldson, D. J., Cziczo, D. J. and Vaida, V.: Processing of
39 unsaturated organic acid films and aerosols by ozone, *Atmos. Environ.*, 37(16), 2207–
40 2219, doi:10.1016/S1352-2310(03)00149-3, 2003.

1 Ervens, B., George, C., Williams, J. E., Buxton, G. V., Salmon, G. A., Bydder, M.,
2 Wilkinson, F., Dentener, F., Mirabel, P., Wolke, R., and Herrmann, H.: CAPRAM 2.4
3 (MODAC mechanism): An extended and condensed tropospheric aqueous phase
4 mechanism and its application, *J. Geophys. Res.*, 108(D14), 4426,
5 doi:10.1029/2002JD002202, 2003.

6 Ervens, B., Carlton, A. G., Turpin, B. J., Altieri, K. E., Kreidenweis, S. M., and Feingold,
7 G.: Secondary organic aerosol yields from cloud processing of isoprene oxidation
8 products, *Geophys. Res. Lett.*, 35, L02816, doi:10.1029/2007gl031828, 2008.

9 Ervens, B. and Volkamer, R.: Glyoxal processing by aerosol multiphase chemistry:
10 towards a kinetic modeling framework of secondary organic aerosol formation in
11 aqueous particles, *Atmos. Chem. Phys.*, 10(17), 8219–8244, doi:10.5194/acp-10-
12 8219-2010, 2010.

13 Ervens, B., Turpin, B. J. and Weber, R. J.: Secondary organic aerosol formation in cloud
14 droplets and aqueous particles (aqSOA): a review of laboratory, field and model
15 studies, *Atmos. Chem. Phys.*, 11(21), 11069–11102, doi:10.5194/acp-11-11069-2011,
16 2011.

17 Falkovich, A. H., Gruber, E. R., Schkolnik, G., Rudich, Y., Maenhaut, W. and Artaxo, P.:
18 Low molecular weight organic acids in aerosol particles from Rondônia, Brazil, during
19 the biomass-burning, transition and wet periods, *Atmos. Chem. Phys.*, 5(3), 781–797,
20 2005.

21 Feng, Y. and Penner, J. E.: Global modeling of nitrate and ammonium: Interaction of
22 aerosols and tropospheric chemistry, *J. Geophys. Res.*, 112, D01304,
23 doi:10.1029/2005JD006404, 2007.

24 Fu, T. M., Jacob, D. J., Wittrock, F., Burrows, J. P., Vrekoussis, M. and Henze, D. K.:
25 Global budgets of atmospheric glyoxal and methylglyoxal, and implications for
26 formation of secondary organic aerosols, *J. Geophys. Res.*, 113, D15303,
27 doi:10.1029/2007jd009505, 2008.

28 Fu, T. M., Jacob, D. J., and Heald, C. L.: Aqueous-phase reactive uptake of dicarbonyls
29 as a source of organic aerosol over eastern North America, *Atmos. Environ.*, 43,
30 1814–1822, 2009.

31 Furukawa, T., and Takahashi, Y.: Oxalate metal complexes in aerosol particles:
32 implications for the hygroscopicity of oxalate-containing particles, *Atmos. Chem.*
33 *Phys.*, 11, 9, 4289-4301, 10.5194/acp-11-4289-2011, 2011.

34

35 Gao, S., Hegg, D. A., Hobbs, P. V., Kirchstetter, T. W., Magi, B. I., and Sadilek, M.:
36 Water-soluble organic components in aerosols associated with savanna fires in
37 southern Africa: Identification, evolution, and distribution, *J. Geophys. Res.*,
38 108(D13), 8491, doi:10.1029/2002JD002324, 2003.

1 Ghan, S. J. and Zaveri, R. A.: Parameterization of optical properties for hydrated
2 internally mixed aerosol, *J. Geophys. Res.*, 112(D10), D10201,
3 doi:10.1029/2006JD007927, 2007.

4 Gilardoni, S., Vignati, E., Marmer, E., Cavalli, F., Belis, C., Gianelle, V., Loureiro, A.
5 and Artaxo, P.: Sources of carbonaceous aerosol in the Amazon basin, *Atmos. Chem.
6 Phys.*, 11(6), 2747–2764, doi:10.5194/acp-11-2747-2011, 2011.

7 Graham, B., Mayol-Bracero, O. L., Guyon, P., Roberts, G. C., Decesari, S., Facchini, M.
8 C., Artaxo, P., Maenhaut, W., Koll, P., and Andreae, M. O.: Water-soluble organic
9 compounds in biomass burning aerosols over Amazonia1. Characterization by NMR
10 and GC-MS, *J. Geophys. Res.*, 107, 8047, doi:10.1029/2001JD000336, 2002.

11 Hack, J. J.: Sensitivity of the Simulated Climate to a Diagnostic Formulation for Cloud
12 Liquid Water, *J. Climate*, 11(7), 1497–1515, 1998.

13 Han, Q., Zender, C. S., Moore, J. K., Buck, C. S., Chen, Y., Johansen, A. and Measures,
14 C. I.: Global estimates of mineral dust aerosol iron and aluminum solubility that
15 account for particle size using diffusion-controlled and surface-area-controlled
16 approximations, *Global Biogeochem. Cycles*, 26(2), GB2038,
17 doi:10.1029/2011GB004186, 2012.

18 He, C., Liu, J., Carlton, A. G. and Fan, S.: Evaluation of factors controlling global
19 secondary organic aerosol production from cloud processes, *Atmos. Chem. Phys.*, 13,
20 1913–1926, 2013.

21 He, N. and Kawamura, K.: Distributions and diurnal changes of low molecular weight
22 organic acids and α -dicarbonyls in suburban aerosols collected at Mangshan, North
23 China, *Geochemical Journal*, 44(4), e17–e22, 2010.

24 Heald, C. L., Jacob, D. J., Park, R. J., Russell, L. M., Huebert, B. J., Seinfeld, J. H., Liao,
25 H., and Weber, R. J.: A large organic aerosol source in the free troposphere missing
26 from current models, *Geophys. Res. Lett.*, 32, L18809, doi:10.1029/2005GL023831,
27 2005.

28 Herrmann, H.: Kinetics of aqueous phase reactions relevant for atmospheric chemistry,
29 *Chem. Rev.*, 103, 4691–4716, 2003.

30 Herrmann, H., Tilgner, A., Barzaghi, P., Majdik, Z., Gligorovski, S., Poulain, L. and
31 Monod, A.: Towards a more detailed description of tropospheric aqueous phase
32 organic chemistry: CAPRAM 3.0, *Atmos. Environ.*, 39(23–24), 4351–4363,
33 doi:10.1016/j.atmosenv.2005.02.016, 2005.

34 Herzog, M., Weisenstein, D. K., and Penner, J. E.: A dynamic aerosol module for global
35 chemical transport models: Model description, *J. Geophys. Res.*, 109, D18202,
36 doi:10.1029/2003JD004405, 2004.

37 Hodzic, A., Jimenez, J. L., Madronich, S., Canagaratna, M. R., DeCarlo, P. F., Kleinman,
38 L. and Fast, J.: Modeling organic aerosols in a megacity: potential contribution of

1 semi-volatile and intermediate volatility primary organic compounds to secondary
2 organic aerosol formation, *Atmos. Chem. Phys.*, 10(12), 5491–5514, doi:10.5194/acp-
3 10-5491-2010, 2010.

4 Ito, A. and Feng, Y.: Role of dust alkalinity in acid mobilization of iron, *Atmos. Chem.*
5 *Phys.*, 10, 9237-9250, doi:10.5194/acp-10-9237-2010, 2010.

6 Ito, A., Sillman, S., and Penner, J. E.: Effects of additional nonmethane volatile organic
7 compounds, organic nitrates, and direct emissions of oxygenated organic species on
8 global tropospheric chemistry, *J. Geophys. Res.*, 112, D06309,
9 doi:10.1029/2005JD006556, 2007.

10 Ito, A., and Xu, L.: Response of acid mobilization of iron-containing mineral dust to
11 improvement of air quality projected in the future, *Atmos. Chem. Phys.*, 14, 3441–
12 3459, doi:10.5194/acp-14-3441-2014, 2014.

13 Jacob, D. J.: Chemistry of OH in remote clouds and its role in the production of formic
14 acid and peroxymonosulfate, *J. Geophys. Res.*, 91(D9), 9807–9826,
15 doi:10.1029/JD091iD09p09807, 1986.

16 Jimenez, J. L., Canagaratna, M. R., Donahue, N. M., Prevot, A. S. H., Zhang, Q., Kroll, J.
17 H., DeCarlo, P. F., Allan, J. D., Coe, H., Ng, N. L., Aiken, A. C., Docherty, K. S.,
18 Ulbrich, I. M., Grieshop, A. P., Robinson, A. L., Duplissy, J., Smith, J. D., Wilson, K.
19 R., Lanz, V. A., Hueglin, C., Sun, Y. L., Tian, J., Laaksonen, A., Raatikainen, T.,
20 Rautiainen, J., Vaattovaara, P., Ehn, M., Kulmala, M., Tomlinson, J. M., Collins, D.
21 R., Cubison, M. J., Dunlea, E. J., Huffman, J. A., Onasch, T. B., Alfarra, M. R.,
22 Williams, P. I., Bower, K., Kondo, Y., Schneider, J., Drewnick, F., Borrmann, S.,
23 Weimer, S., Demerjian, K., Salcedo, D., Cottrell, L., Griffin, R., Takami, A., Miyoshi,
24 T., Hatakeyama, S., Shimono, A., Sun, J. Y., Zhang, Y. M., Dzepina, K., Kimmel, J.
25 R., Sueper, D., Jayne, J. T., Herndon, S. C., Trimborn, A. M., Williams, L. R., Wood,
26 E. C., Middlebrook, A. M., Kolb, C. E., Baltensperger, U., and Worsnop, D. R.:
27 Evolution of Organic Aerosols in the Atmosphere, *Science*, 326, 1525–1529, 2009.

28 Johnson, M. S. and Meskhidze, N.: Atmospheric dissolved iron deposition to the global
29 oceans: effects of oxalate-promoted Fe dissolution, photochemical redox cycling, and
30 dust mineralogy, *Geosci. Model Dev.*, 6, 1137–1155, doi:10.5194/gmd-6-1137-2013,
31 2013.

32 Kampf, C. J., Waxman, E. M., Slowik, J. G., Dommen, J., Pfaffenberger, L., Praplan, A.
33 P., Prevot, A. S. H., Baltensperger, U., Hoffmann, T., and Volkamer, R.: Effective
34 Henry's law partitioning and the salting constant of glyoxal in aerosols containing
35 sulfate, *Environ. Sci. Technol.*, 43, 4236–4244, 2013.

36 Kundu, S., Kawamura, K., Lee, M., Andreae, T. W., Hoffer, A. and Andreae, M. O.:
37 Comparison of Amazonian biomass burning and East Asian marine aerosols: Bulk
38 organics, diacids and related compounds, water-soluble inorganic ions, stable carbon
39 and nitrogen isotope ratios, *Low Temp. Sci.*, 68, 89–100, 2010.

1 Lee-Taylor, J., Madronich, S., Aumont, B., Baker, A., Camredon, M., Hodzic, A.,
2 Tyndall, G. S., Apel, E., and Zaveri, R. A.: Explicit modeling of organic chemistry
3 and secondary organic aerosol partitioning for Mexico City and its outflow plume,
4 *Atmos. Chem. Phys.*, 11, 13219-13241, doi:10.5194/acp-11-13219-2011, 2011.
5

6 Legrand, M., Preunkert, S., Oliveira, T., Pio, C. A., Hammer, S., Gelencsér, A., Kasper-
7 Giebl, A. and Laj, P.: Origin of C₂–C₅ dicarboxylic acids in the European atmosphere
8 inferred from year-round aerosol study conducted at a west-east transect, *J. Geophys.*
9 *Res.*, 112(D23), D23S07, doi:10.1029/2006JD008019, 2007.

10 Lelieveld, J. and Crutzen, P. J.: The role of clouds in tropospheric photochemistry, *J*
11 *Atmos Chem*, 12(3), 229–267, doi:10.1007/BF00048075, 1991.

12 Liggio, J., Li, S. M. and McLaren, R.: Heterogeneous reactions of glyoxal on particulate
13 matter: Identification of acetals and sulfate esters, *Environ. Sci. Technol.*, 39(6),
14 1532–1541, 2005.

15 Lim, H. J., Carlton, A. G. and Turpin, B. J.: Isoprene forms secondary organic aerosol
16 through cloud processing: model simulations, *Environ. Sci. Technol.*, 9(12), 4441-
17 4446, 2005.

18 Lim, Y. B., Tan, Y., Perri, M. J., Seitzinger, S. P. and Turpin, B. J.: Aqueous chemistry
19 and its role in secondary organic aerosol (SOA) formation, *Atmos. Chem. Phys.*,
20 10(21), 10521–10539, doi:10.5194/acp-10-10521-2010, 2010.

21 Lim, Y. B., Tan, Y. and Turpin, B. J.: Chemical insights, explicit chemistry and yields of
22 secondary organic aerosol from methylglyoxal and glyoxal, *Atmos. Chem. Phys.*, 13,
23 8651–8667, doi:10.5194/acpd-13-8651-2013, 2013.

24 Lin, G., Penner, J. E., Sillman, S., Taraborrelli, D. and Lelieveld, J.: Global modeling of
25 SOA formation from dicarbonyls, epoxides, organic nitrates and peroxides, *Atmos.*
26 *Chem. Phys.*, 12(10), 4743–4774, doi:10.5194/acp-12-4743-2012, 2012.

27 Liu, J., Horowitz, L. W., Fan, S., Carlton, A. G. and Levy, H., II: Global in-cloud
28 production of secondary organic aerosols: Implementation of a detailed chemical
29 mechanism in the GFDL atmospheric model AM3, *J. Geophys. Res.*, 117(D15),
30 D15303, doi:10.1029/2012JD017838, 2012.

31 Liu, S., Shilling, J. E., Song, C., Hiranuma, N., Zaveri, R. A., and Russell, L. M.:
32 Hydrolysis of organonitrate functional groups in aerosol particles, *Aerosol Sci.*
33 *Technol.*, 46, 1359–1369, 2012.

34 Liu, X. H. and Penner, J. E.: Effect of Mount Pinatubo H₂SO₄/H₂O aerosol on ice
35 nucleation in the upper troposphere using a global chemistry and transport model, *J.*
36 *Geophys. Res.*, 107, 4141-4157, doi:10.1029/2001JD000455, 2002.

37 Liu, X. H., Penner, J. E. and Herzog, M.: Global modeling of aerosol dynamics: Model
38 description, evaluation, and interactions between sulfate and nonsulfate aerosols, *J.*
39 *Geophys. Res.*, 110, D18206, doi:10.1029/2004jd005674, 2005.

1 Liu, X., Mauersberger, G. and Möller, D.: The effects of cloud processes on the
2 tropospheric photochemistry: An improvement of the eurad model with a coupled
3 gaseous and aqueous chemical mechanism, *Atmos. Environ.*, 31(19), 3119–3135,
4 doi:10.1016/S1352-2310(97)00057-5, 1997.

5 Myriokefalitakis, S., Tsigaridis, K., Mihalopoulos, N., Sciare, J., Nenes, A., Kawamura,
6 K., Segers, A., and Kanakidou, M.: In-cloud oxalate formation in the global
7 troposphere: a 3-D modeling study, *Atmos. Chem. Phys.*, 11, doi:10.5194/acp-11-
8 5761-2011, 5761–5782, 2011.

9 Ng, N. L., Chhabra, P. S., Chan, A. W. H., Surratt, J. D., Kroll, J. H., Kwan, A. J.,
10 McCabe, D. C., Wennberg, P. O., Sorooshian, A., Murphy, S. M., Dalleska, N. F.,
11 Flagan, R. C., and Seinfeld, J. H.: Effect of NO_x level on secondary organic aerosol
12 (SOA) formation from the photooxidation of terpenes, *Atmos. Chem. Phys.*, 7, 5159–
13 5174, doi:10.5194/acp-7-5159-2007, 2007.

14 Ng, N. L., Canagaratna, M. R., Zhang, Q., Jimenez, J. L., Tian, J., Ulbrich, I. M., Kroll, J.
15 H., Docherty, K. S., Chhabra, P. S., Bahreini, R., Murphy, S. M., et al.: Organic
16 aerosol components observed in Northern Hemispheric datasets from Aerosol Mass
17 Spectrometry, *Atmos. Chem. Phys.*, 10(10), 4625–4641, doi:10.5194/acp-10-4625-
18 2010, 2010.

19 Odum, J. R., Hoffmann, T., Bowman, F., Collins, D., Flagan, R. C. and Seinfeld, J. H.:
20 Gas/particle partitioning and secondary organic aerosol yields, *Environ. Sci. Technol.*,
21 30(8), 2580–2585, 1996.

22 Pandis, S. N. and Seinfeld, J. H.: Sensitivity analysis of a chemical mechanism for
23 aqueous-phase atmospheric chemistry, *J. Geophys. Res.*, 94, 1105-1126,
24 doi:10.1029/JD094iD01p01105, 1989.

25 Pankow, J. F.: An absorption model of gas/particle partitioning of organic compounds in
26 the atmosphere, *Atmos. Environ.*, 28(2), 185–188, doi:10.1016/1352-2310(94)90093-
27 0, 1994.

28 Paulot, F., Crounse, J. D., Kjaergaard, H. G., Kurten, A., St Clair, J. M., Seinfeld, J. H.
29 and Wennberg, P. O.: Unexpected Epoxide Formation in the Gas-Phase
30 Photooxidation of Isoprene, *Science*, 325(5941), 730–733,
31 doi:10.1126/science.1172910, 2009.

32 Peeters, J., Nguyen, T. L. and Vereecken, L.: HO_x radical regeneration in the oxidation
33 of isoprene, *Physical Chemistry Chemical Physics*, 11(28), 5935–5939,
34 doi:10.1039/b908511d, 2009.

35 Penner, J. E., Chuang, C. C. and Grant, K.: Climate forcing by carbonaceous and sulfate
36 aerosols, *Climate Dynamics*, 14(12), 839–851, 1998.

37 Perri, M. J., Seitzinger, S., and Turpin, B. J.: Secondary organic aerosol production from
38 aqueous photooxidation of glycolaldehyde: Laboratory experiments, *Atmos. Environ.*,
39 43, 1487–1497, 2009.

1 Pye, H. O. T. and Seinfeld, J. H.: A global perspective on aerosol from low-volatility
2 organic compounds, *Atmos. Chem. Phys.*, 10(9), 4377–4401, doi:10.5194/acp-10-
3 4377-2010, 2010.

4 Rinaldi, M., Decesari, S., Carbone, C., Finessi, E., Fuzzi, S., Ceburnis, D., O'Dowd, C.,
5 Sciare, J., Burrows, J., Vrekoussis, M., Ervens, B., Tsigaridis, K., and Facchini, M. C.:
6 Evidence of a natural marine source of oxalic acid and a possible link to glyoxal, *J. Geophys. Res.*, 116, D16204, doi:10.1029/2011JD015659. 2011.

8 Robinson, A. L., Donahue, N. M., Shrivastava, M. K., Weitkamp, E. A., Sage, A. M.,
9 Grieshop, A. P., Lane, T. E., Pierce, J. R. and Pandis, S. N.: Rethinking organic
10 aerosols: Semivolatile emissions and photochemical aging, *Science*, 315(5816), 1259–
11 1262, doi:10.1126/science.1133061, 2007.

12 Robinson, N. H., Hamilton, J. F., Allan, J. D., Langford, B., Oram, D. E., Chen, Q.,
13 Docherty, K., Farmer, D. K., Jimenez, J. L., Ward, M. W., Hewitt, C. N., Barley, M.
14 H., Jenkin, M. E., Rickard, A. R., Martin, S. T., McFiggans, G., and Coe, H.: Evidence
15 for a significant proportion of Secondary Organic Aerosol from isoprene above a
16 maritime tropical forest, *Atmos. Chem. Phys.*, 11, 1039–1050, doi:10.5194/acp-11-
17 1039-2011, 2011.

18 Schwartz, S. E.: Mass-transport considerations pertinent to aqueous phase reactions of
19 gases on liquid water clouds, in *Chemistry of Multiphase Atmospheric Systems*,
20 NATO ASI Ser., edited by: Jaeschke, W., Springer, Berlin, Germany, 1986.

21 Sillman, S.: A numerical-solution for the equations of tropospheric chemistry based on an
22 analysis of sources and sinks of odd hydrogen, *J. Geophys. Res.*, 96(D11), 20735–
23 20744, 1991.

24 Sillman, S., Marsik, F. J., Al-Wali, K. I., Keeler, G. J. and Landis, M. S.: Reactive
25 mercury in the troposphere: Model formation and results for Florida, the northeastern
26 United States, and the Atlantic Ocean, *J. Geophys. Res.*, 112(D23), D23305,
27 doi:10.1029/2006JD008227, 2007.

28 Smith, M. L., Bertram, A. K. and Martin, S. T.: Deliquescence, efflorescence, and phase
29 miscibility of mixed particles of ammonium sulfate and isoprene-derived secondary
30 organic material, *Atmos. Chem. Phys.*, 12, 9613–9628, doi:10.5194/acp-12-9613-
31 2012, 2012.

32 Sorooshian, A., Brechtel, F. J., Ervens, B., Feingold, G., Varutbangkul, V., Bahreini, R.,
33 Murphy, S., Holloway, J. S., Atlas, E. L., Anlauf, K., Buzorius, G., Jonsson, H.,
34 Flagan, R. C., and Seinfeld, J. H.: Oxalic acid in clear and cloudy atmospheres:
35 Analysis of data from International Consortium for Atmospheric Research on
36 Transport and Transformation 2004, *J. Geophys. Res.*, 111, D23,
37 doi:10.1029/2005JD006880, 2006.

39 Sorooshian, A., Wang, Z., Coggon, M. M., Jonsson, H. H., and Ervens, B.: Observations
40 of Sharp Oxalate Reductions in Stratocumulus Clouds at Variable Altitudes: Organic

1 Acid and Metal Measurements During the 2011 E-PEACE Campaign, *Environ. Sci.
2 Technol.*, 47, 14,7747-7756, 10.1021/es4012383, 2013.
3

4 Sorooshian, A., Lu, M. L., Brechtel, F. J., Jonsson, H., Feingold, G., Flagan, R. C., and
5 Seinfeld, J. H.: On the source of organic acid aerosol layers above clouds, *Environ.
6 Sci. Technol.*, 41, 4647–4654, 2007.

7 Spracklen, D. V., Jimenez, J. L., Carslaw, K. S., Worsnop, D. R., Evans, M. J., Mann, G.
8 W., Zhang, Q., Canagaratna, M. R., Allan, J., Coe, H., McFiggans, G., Rap, A., and
9 Forster, P.: Aerosol mass spectrometer constraint on the global secondary organic
10 aerosol budget, *Atmos. Chem. Phys.*, 11, 12109–12136, doi:10.5194/acp-11-12109-
11 2011, 2011.

12 Stavrakou, T., Muller, J. F., De Smedt, I., Van Roozendael, M., Kanakidou, M.,
13 Vrekoussis, M., Wittrock, F., Richter, A. and Burrows, J. P.: The continental source of
14 glyoxal estimated by the synergistic use of spaceborne measurements and inverse
15 modelling, *Atmos. Chem. Phys.*, 9(21), 8431–8446, 2009.

16 Sundqvist, H., Berge, E. and Kristjánsson, J. E.: Condensation and Cloud
17 Parameterization Studies with a Mesoscale Numerical Weather Prediction Model,
18 *Mon. Wea. Rev.*, 117(8), 1641–1657, 1989.

19 Surratt, J. D., Chan, A. W. H., Eddingsaas, N. C., Chan, M. N., Loza, C. L., Kwan, A. J.,
20 Hersey, S. P., Flagan, R. C., Wennberg, P. O. and Seinfeld, J. H.: Reactive
21 intermediates revealed in secondary organic aerosol formation from isoprene, *Proc.
22 Natl. Acad. Sci. USA.*, 107(15), 6640–6645, doi:10.1073/pnas.0911114107, 2010.

23 Talbot, R. W., Andreae, M. O., Andreae, T. W. and Harriss, R. C.: Regional aerosol
24 chemistry of the Amazon Basin during the dry season, *J. Geophys. Res.*, 93(D2),
25 1499, doi:10.1029/JD093iD02p01499, 1988.

26 Taylor, S. R. and McLennan S. M.: *The Continental Crust: Its Composition and
27 Evolution*, 312 pp., Blackwell Sci., Oxford, U.K., 1985.

28 Tan, Y., Perri, M. J., Seitzinger, S. P. and Turpin, B. J.: Effects of Precursor
29 Concentration and Acidic Sulfate in Aqueous Glyoxal–OH Radical Oxidation and
30 Implications for Secondary Organic Aerosol, *Environ. Sci. Technol.*, 43(21), 8105–
31 8112, doi:10.1021/es901742f, 2009.

32 Tan, Y., Carlton, A. G., Seitzinger, S. P., and Turpin, B. J.: SOA from methylglyoxal in
33 clouds and wet aerosols: Measurement and prediction of key products, *Atmos.
34 Environ.*, 44, 5218–5226, 2010.

35 Tan, Y., Lim, Y. B., Altieri, K. E., Seitzinger, S. P. and Turpin, B. J.: Mechanisms
36 leading to oligomers and SOA through aqueous photooxidation: insights from OH
37 radical oxidation of acetic acid and methylglyoxal, *Atmos. Chem. Phys.*, 12(2), 801–
38 813, doi:10.5194/acp-12-801-2012, 2012.

1 Volkamer, R., Jimenez, J. L., SanMartini, F., Dzepina, K., Zhang, Q., Salcedo, D.,
2 Molina, L. T., Worsnop, D. R., and Molina, M. J.: Secondary organic aerosol
3 formation from anthropogenic air pollution: Rapid and higher than expected, *Geophys.*
4 *Res. Lett.*, 33, L17811, doi:10.1029/2006GL026899, 2006.

5 Volkamer, R., Ziemann, P. J., and Molina, M. J.: Secondary Organic Aerosol Formation
6 from Acetylene (C₂H₂): seed effect on SOA yields due to organic photochemistry in
7 the aerosol aqueous phase, *Atmos. Chem. Phys.*, 9, 1907–1928, doi:10.5194/acp- 9-
8 1907-2009, 2009.

9 Wang, G., Kawamura, K., Umemoto, N., Xie, M., Hu, S. and Wang, Z.: Water-soluble
10 organic compounds in PM 2.5 and size-segregated aerosols over Mount Tai in North
11 China Plain, *J. Geophys. Res.*, 114(D19), D19208, doi:10.1029/2008JD011390, 2009.

12 Wang, M. H., Penner, J. E., and Liu, X. H.: Coupled IMPACT aerosol and NCAR CAM3
13 model: Evaluation of predicted aerosol number and size distribution, *J. Geophys. Res.*,
14 114, D06302, doi:10.1029/2008JD010459, 2009.

15 Warneke, P.: In-cloud chemistry opens pathway to the formation of oxalic acid in the
16 marine atmosphere, *Atmos. Environ.*, 37(17), 2423–2427, doi:10.1016/S1352-
17 2310(03)00136-5, 2003.

18 Waxman, E. M., Dzepina, K., Ervens, B., Lee-Taylor, J., Aumont, B., Jimenez, J. L.,
19 Madronich, S. and Volkamer, R.: Secondary organic aerosol formation from semi- and
20 intermediate-volatility organic compounds and glyoxal: Relevance of O/C as a tracer
21 for aqueous multiphase chemistry, *Geophys. Res. Lett.*, 40, 978–982,
22 doi:10.1002/grl.50203, 2013.

23 Wonaschuetz, A., Sorooshian, A., Ervens, B., Chuang, P. Y., Feingold, G., Murphy, S.
24 M., de Gouw, J., Warneke, C., and Jonsson, H. H.: Aerosol and gas redistribution by
25 shallow cumulus clouds: An investigation using airborne measurements, *J. Geophys.*
26 *Res.*, 117, D17, D17202, 10.1029/2012jd018089, 2012.

27

28 Xing, L., Fu, T. M., Cao, J. J., Lee, S. C., Wang, G. H., Ho, K. F., Cheng, M. C., You, C.
29 F. and Wang, T. J.: Seasonal and spatial variability of the OM/OC mass ratios and
30 high regional correlation between oxalic acid and zinc in Chinese urban organic
31 aerosols, *Atmos. Chem. Phys.*, 13, 4307–4318, doi:10.5194/acp-13-4307-2013, 2013.

32 Xu, K.-M. and Krueger, S. K.: Evaluation of Cloudiness Parameterizations Using a
33 Cumulus Ensemble Model, *Mon. Wea. Rev.*, 119(2), 342–367, doi:10.1175/1520-
34 0493, 1991.

35 Xu, L. and Penner, J. E.: Global simulations of nitrate and ammonium aerosols and their
36 radiative effects, *Atmos. Chem. Phys.*, 12, 9479-9504, doi:10.5194/acp-12-9479-2012,
37 2012.

38 Zhang, Q., Jimenez, J. L., Canagaratna, M. R., Allan, J. D., Coe, H., Ulbrich, I., Alfarra,
39 M. R., Takami, A., Middlebrook, A. M., Sun, Y. L., Dzepina, K., Dunlea, E.,
40 Docherty, K., DeCarlo, P. F., Salcedo, D., Onasch, T., Jayne, J. T., Miyoshi, T.,

1 Shimono, A., Hatakeyama, S., Takegawa, N., Kondo, Y., Schneider, J., Drewnick, F.,
2 Borrmann, S., Weimer, S., Demerjian, K., Williams, P., Bower, K., Bahreini, R.,
3 Cottrell, L., Griffin, R. J., Rautiainen, J., Sun, J. Y., Zhang, Y. M., and Worsnop, D.
4 R.: Ubiquity and dominance of oxygenated species in organic aerosols in
5 anthropogenically-influenced Northern Hemisphere midlatitudes, *Geophys. Res. Lett.*,
6 34, L13801, doi:10.1029/2007GL029979, 2007.

Table 1. Case descriptions

Case name	SOA formation in cloud water	SOA formation in aerosol water	Cloud field	Iron chemistry
Case 1	Multiphase reaction scheme is used to predict carboxylic acids and a kinetic approach is used for all gas/particle transfer. Aqueous phase reactions of organics are adopted from Jacob (1986), Pandis and Seinfeld (1989), Lim et al. (2005), Herrmann (2003), and Herrmann et al. (2005) (Table S3 in the Supplement)	Multiphase reaction scheme is used to predict carboxylic acids with the same aqueous phase reactions and gas/particle transfer as in cloud water. Surface-limited uptake process is used to predict oligomers with a reactive uptake parameter of 3.3E-3 for glyoxal and 2.9E-5 for methylglyoxal	The diagnostic cloud field ^a	N/A
Case 2	The same as in Case 1	Multiphase reaction scheme is used with the aqueous phase reactions proposed by Ervens and Volkamer (2010) (Table S4 in the Supplement)	The diagnostic cloud field ^a	N/A
Case 3	Multiphase reaction scheme is used with the detailed chemistry of Lim et al. (2010) (Table S5 in the Supplement)	Multiphase reaction scheme is used with the detailed chemistry of Lim et al. (2010) (Table S5 in the Supplement)	The diagnostic cloud field ^a	N/A
Case 4	The same as in Case 1	The same as in Case 1	GFDL AM3 cloud field	N/A
Case 5	The same as in Case 1, but including aqueous iron chemistry in cloud (Table S6 in the Supplement)	The same as in Case 1	The diagnostic cloud field ^a	Includes aqueous iron chemistry
Case 6	Surface-limited uptake process is used with a reactive uptake parameter of 2.9E-3 for both glyoxal and methylglyoxal	Surface-limited uptake process is used with a reactive uptake parameter of 2.9E-3 for both glyoxal and methylglyoxal	The diagnostic cloud field ^a	N/A

^aThe diagnostic cloud field used the parameterization for cloud water published by Hack (1998)

Table 2. Global aqSOA budget analyses for all cases

Case name	Species name	Chemical production (Tg/yr)	Chemical destruction (Tg/yr)	Net production (Tg/yr)	Dry deposition (Tg/yr)	Wet deposition (Tg/yr)	Burden (Tg)
Case 1	Glyoxylic acid	15.9	13.5	2.4	0.1	2.3	1.8×10^{-2}
	Pyruvic acid	7.2×10^{-1}	5.5×10^{-1}	1.7×10^{-1}	1.0×10^{-2}	1.6×10^{-1}	1.1×10^{-3}
	Oxalic acid	16.5	6.1	10.4	0.5	9.9	6.1×10^{-2}
	Glyoxal oligomer	6.9	--	6.9	0.4	6.5	9.2×10^{-2}
	Methylglyoxal oligomer	2.3×10^{-1}	--	2.3×10^{-1}	2.4×10^{-2}	2.0×10^{-1}	2.3×10^{-3}
Case 2	Glyoxylic acid	16.5	13.9	2.6	0.1	2.5	1.8×10^{-2}
	Pyruvic acid	7.0×10^{-1}	5.3×10^{-1}	1.7×10^{-1}	7.8×10^{-3}	1.6×10^{-1}	1.1×10^{-3}
	Oxalic acid	16.9	6.3	10.6	0.4	10.2	6.4×10^{-2}
	Glyoxal oligomer	2.8×10^{-2}	--	2.8×10^{-2}	5.1×10^{-3}	2.3×10^{-2}	2.1×10^{-3}
	Methylglyoxal oligomer	1.7×10^{-2}	--	1.7×10^{-2}	4.4×10^{-3}	1.3×10^{-2}	9.7×10^{-4}
Case 3	Glyoxylic acid	14.8	12.3	2.5	0.1	2.4	1.8×10^{-2}
	Pyruvic acid	6.0×10^{-1}	4.4×10^{-1}	1.6×10^{-1}	7.8×10^{-3}	1.5×10^{-1}	1.1×10^{-3}
	Oxalic acid	15.0	5.0	10.0	0.3	9.7	6.1×10^{-2}
	Glyoxal oligomer	1.1×10^{-1}	7.5×10^{-2}	3.4×10^{-2}	2.6×10^{-3}	3.1×10^{-2}	2.7×10^{-3}
	Methylglyoxal oligomer	1.5×10^{-3}	--	1.5×10^{-3}	8.2×10^{-5}	1.4×10^{-3}	1.2×10^{-4}
Case 4	Glyoxylic acid	8.4	7.4	1.0	0.1	0.9	1.4×10^{-2}
	Pyruvic acid	4.5×10^{-1}	3.6×10^{-1}	9.0×10^{-2}	6.0×10^{-3}	8.0×10^{-2}	1.2×10^{-3}
	Oxalic acid	9.0	4.9	4.1	0.3	3.8	5.5×10^{-2}
	Glyoxal oligomer	9.7	--	9.7	0.9	8.8	1.3×10^{-1}
	Methylglyoxal oligomer	4.0×10^{-1}	--	4.0×10^{-1}	5.7×10^{-2}	3.4×10^{-1}	5.0×10^{-3}
Case 5	Glyoxylic acid	23.0	20.6	2.4	0.1	2.3	1.5×10^{-2}
	Pyruvic acid	1.8	1.6	0.2	1.0×10^{-2}	1.9×10^{-1}	1.3×10^{-3}
	Oxalic acid	27.3	22.9	4.4	0.2	4.4	4.7×10^{-2}
	Glyoxal oligomer	6.6	--	6.6	0.4	6.2	8.7×10^{-2}
	Methylglyoxal oligomer	2.3×10^{-1}	--	2.3×10^{-1}	2.5×10^{-2}	2.0×10^{-1}	2.3×10^{-3}
Case 6	Glyoxal oligomer	22.6	--	22.6	1.0	21.6	2.0×10^{-1}
	Methylglyoxal oligomer	36.9	--	36.9	1.6	35.3	3.0×10^{-1}

Table 3. Predicted global average production rates in cloud water by the individual reactions for Case 1^a

	Source	Reaction rate (Tg/yr)	Sink	Reaction rate (Tg/yr)
Glyoxylic acid	Glyoxal + OH/NO ₃	12.2	Reaction with OH	12.7
	Methylglyoxal +OH/NO ₃	6.5×10 ⁻²	Reaction with NO ₃	
	Acetic acid + OH	1.3		
	Glycolaldehyde +OH	2.2		7.2×10 ⁻¹
Oxalic acid	Glyoxylic acid +OH	14.6	Reaction with OH	3.5
	Glyoxylic acid + NO ₃	8.7×10 ⁻¹	Reaction with NO ₃	1.1
Pyruvic acid	Methylglyoxal + OH	7.0×10 ⁻¹	Reaction with OH	5.2×10 ⁻¹
	Methylglyoxal + NO ₃	1.5×10 ⁻²	Reaction with NO ₃	1.4×10 ⁻³

^a organic acids formed in cloud water account for around 67% of total aqSOA formation rate, while the rest is attributed to the oligomer formation in aerosol water.

Table 4. Global budgets of aqSOA precursors (Tg/yr) for Case 1

	Glyoxal	Methylglyoxal	Glycolaldehyde	Acetic Acid
Emission	0	0	0	31.4
Gas phase production	69.6	167.3	81.5	29.5
Aqueous phase production	3.4	0	0	3.8×10 ⁻¹
Gas phase consumption	47.7	158.0	63.7	25.9
Aqueous phase consumption	17.0	0.88	5.3	1.2
Deposition	8.3	9.3	12.5	34.2

Table 5. aqSOA formation in cloud vs. aqSOA formation in aerosol water

	SOA production rate in cloud (Tg/yr)	SOA production rate in aerosol water (Tg/yr)	Total aqSOA production rate (Tg/yr)	Fraction of SOA production in cloud
Case 1	13.4	6.7	20.1	66.7%
Case 2	13.8	-0.4	13.4	103.0%
Case 3	13.1	-0.4	12.7	103.2%
Case 4	6.8	8.5	15.3	44.4%
Case 5	7.3	6.5	13.8	52.9%
Case 6	46.8	12.6	59.4	78.8%

Table 6. Normalized mean bias (NMB) and correlation coefficient (R) between the predicted SOA for the simulations and observations reported by Zhang et al. (2007). The number of sites in the comparison is in parentheses.

Case name	Urban sites (N=14)		Urban downwind sites (N=6)		Rural sites (N=17)	
	NMB	R	NMB	R	NMB	R
Case 1	-40.3%	0.69	-37.6%	0.87	-32.4%	0.24
Case 2	-49.2%	0.71	-48.0%	0.90	-42.5%	0.28
Case 3	-49.5%	0.72	-48.3%	0.89	-42.9%	0.28
Case 4	-28.1%	0.63	-25.9%	0.80	-13.8%	0.25
Case 5	-41.2%	0.69	-38.4%	0.85	-33.2%	0.24
Case 6	-12.5%	0.72	+8.9%	0.86	+20.0%	0.30

Table 7. Comparison of simulated OA and NO_x with observations in tropical forested regions.

	West Africa (Below 2 km)		Amazon Basin (surface)	Malaysian Borneo (surface)
	NO _x (ppt)	SOA (μg/m ³)	Total OA (μg/m ³)	Total OA (μg/m ³)
Observations	210 (Capes et al., 2009)	1.18 (Capes et al., 2009)	0.7 (Chen et al., 2009) 1.70 (Gilardoni et al., 2011)	0.74 (Robinson et al., 2011)
Simulations	Case 1	354	2.54	1.10
	Case 2	354	2.36	0.87
	Case 3	352	2.20	0.80
	Case 4	367	2.69	1.07
	Case 5	347	1.90	0.84
	Case 6	352	4.47	1.57

Table 8. Comparison of the normalized mean bias (NMB) between observations and the model results for different cases.

	AMS measurements at rural sites in Northern Hemisphere ¹	AMS measurements in tropical regions ²	Oxalate measurements ³
Case 1	-32.4%	70.7%	-63.1%
Case 2	-42.5%	49.7%	-61.2%
Case 3	-42.9%	38.7%	-62.2%
Case 4	-13.8%	82.9%	-76.2%
Case 5	-33.2%	19.3%	-88.2%
Case 6	+20.0%	189.7%	N/A

¹ reported by Zhang et al. (2007)

² reported by Capes et al. (2009), Gilardoni et al. (2011), and Robinson et al. (2011)

³ compiled by Myriokefalitakis et al. (2011)

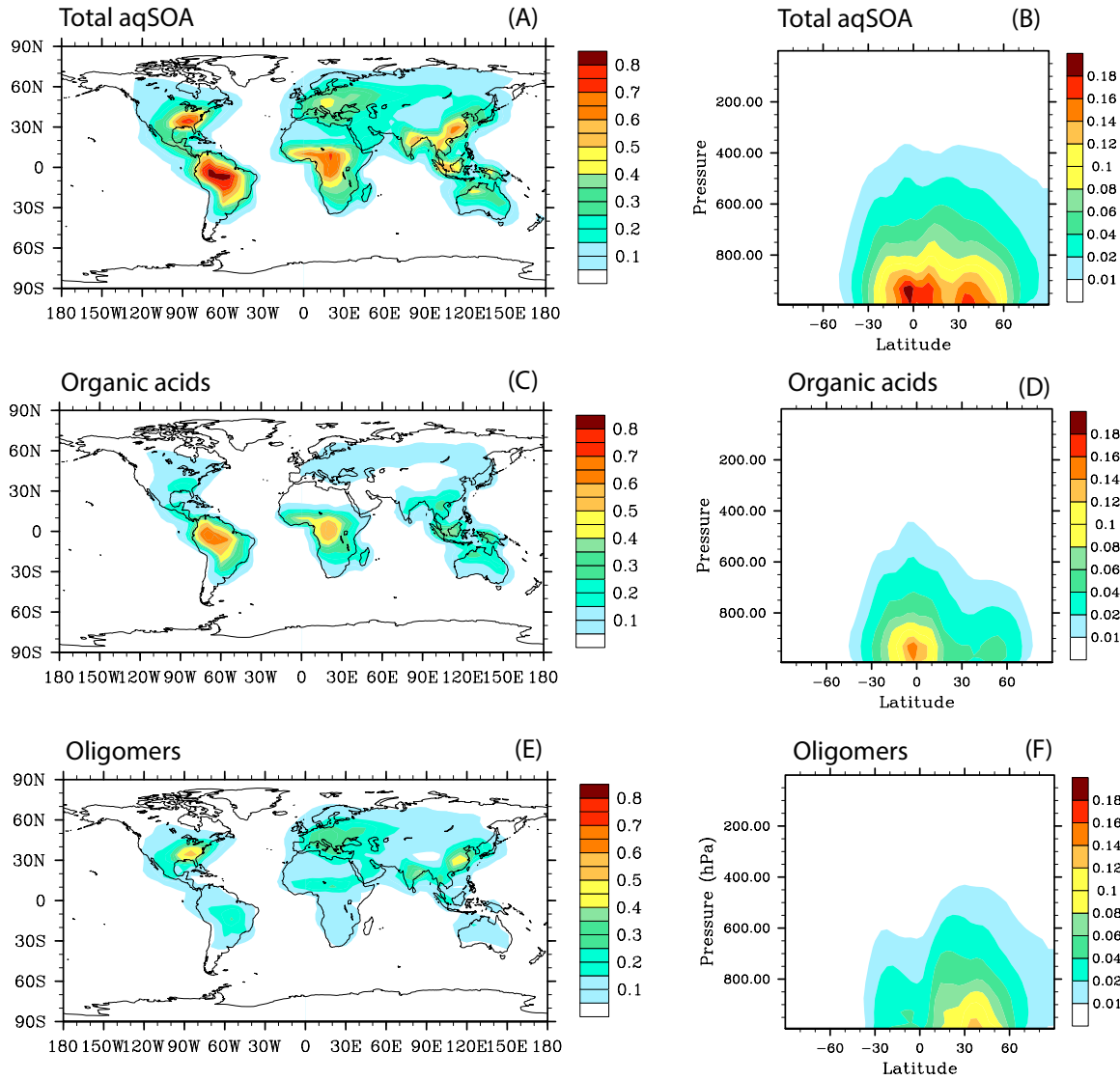


Figure 1. Annual mean simulated concentrations of total aqSOA (panel A and B), organic acids (the sum of glyoxylic acid, pyruvic acid and oxalic acid) (panels C and D), and oligomers from glyoxal and methylglyoxal (panels E and F). The left column shows the global distributions at the level of 971 hPa in the model; the right column depicts the zonal mean distributions. All plots are for Case 1. Units: $\mu\text{g}/\text{m}^3$.

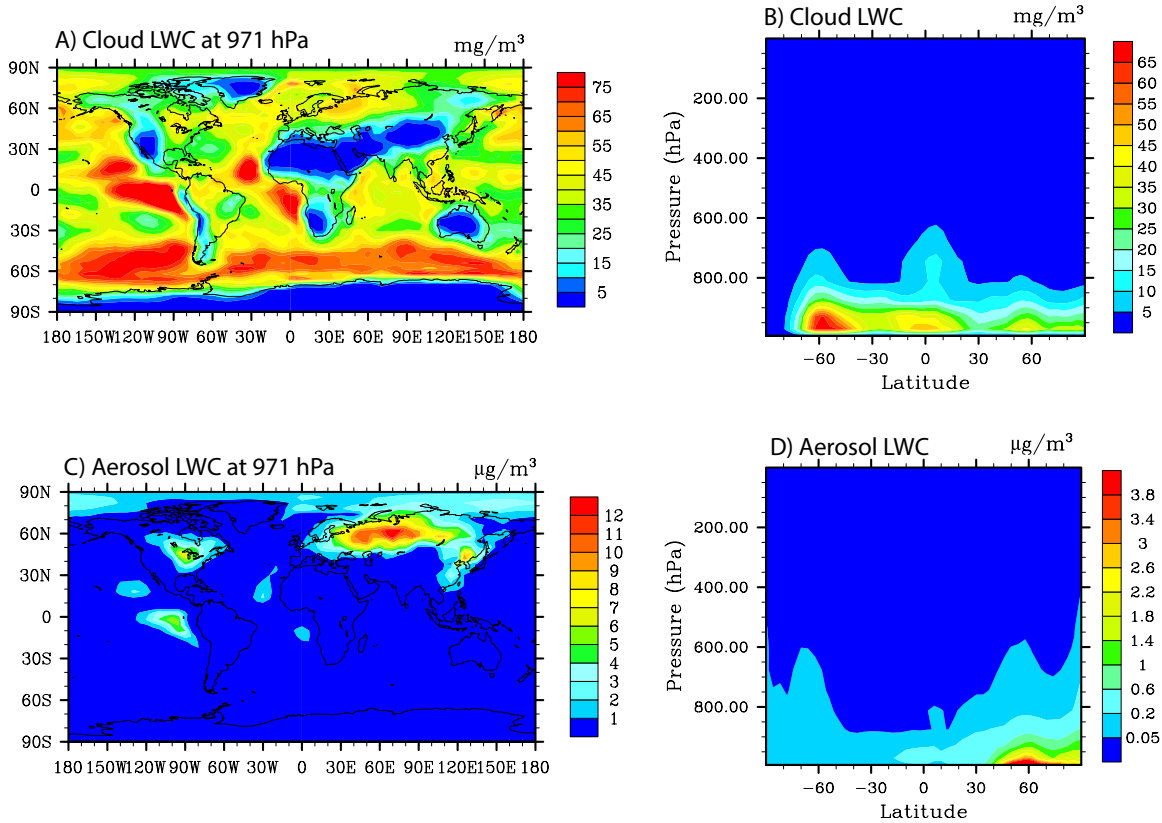


Figure 2. Annual mean grid-box averaged cloud liquid water content (LWC) in mg/m^3 at approximately 971 hPa (A) and zonal mean content (B), and annual mean aerosol LWC in $\mu\text{g/m}^3$ at approximately 971 hPa (C) and zonal mean content (D). Plots are for Case 1, but are the same for all cases except Case 4 (compare Figure 4).

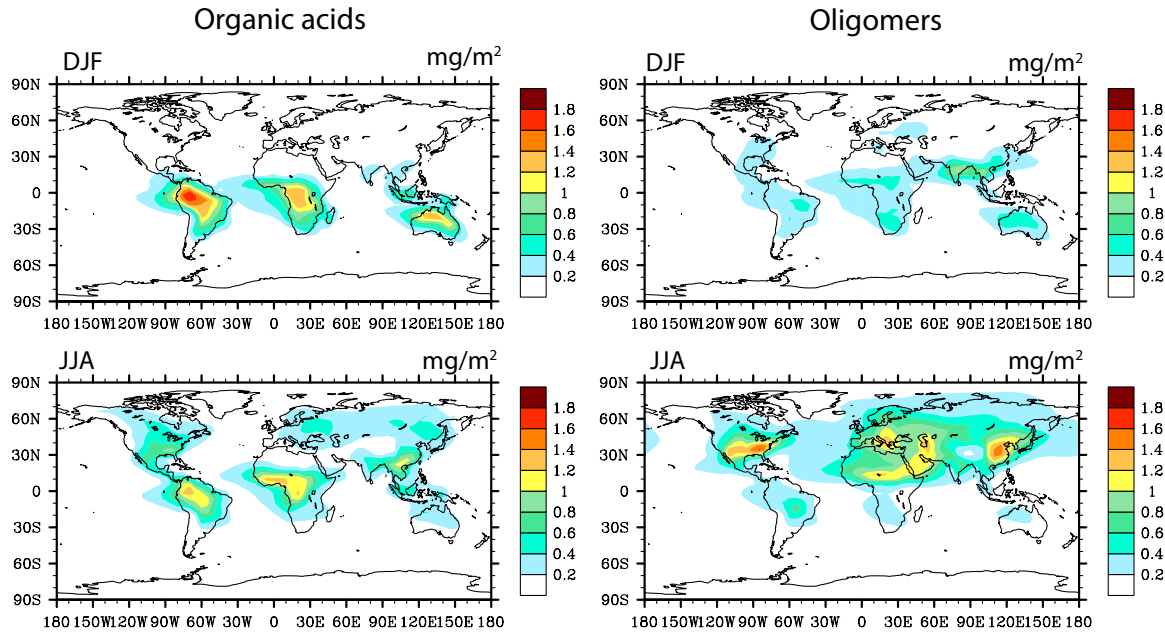


Figure 3. Seasonally averaged column concentrations (mg/m^2) of organic acids (left column) and oligomers (right column) in December, January and February (DJF) (top row) and in June, July and August (JJA) (bottom row). All plots are for Case 1.

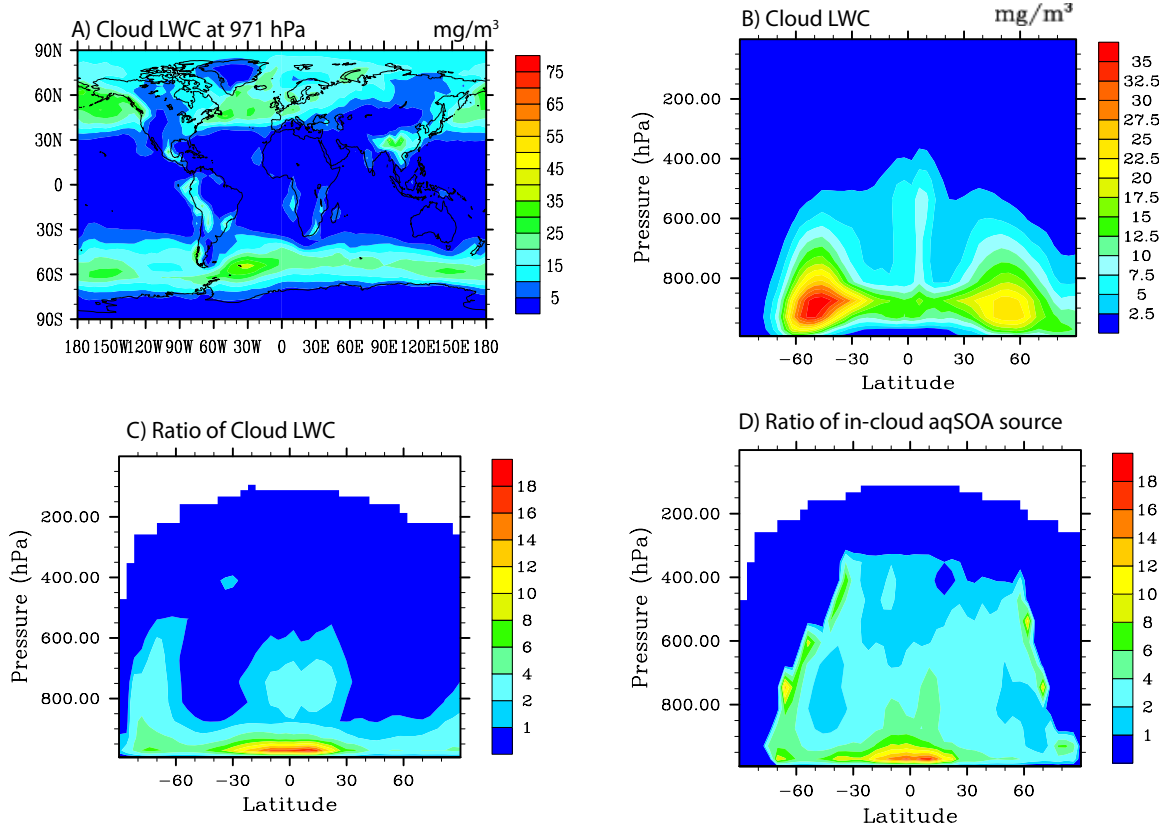


Figure 4. Annual mean grid-box averaged cloud liquid water content (LWC) in mg/m^3 from the GFDL AM3 cloud field at approximately 971 hPa (A) and zonal mean content (B) for Case 4. Panel C shows the zonal mean distributions for the ratio of grid-box averaged cloud LWC in Case 1 to that in Case 4; panel D shows the zonal mean distributions for the ratio of the source of aqSOA formed in cloud water in Case 1 to that in Case 4.

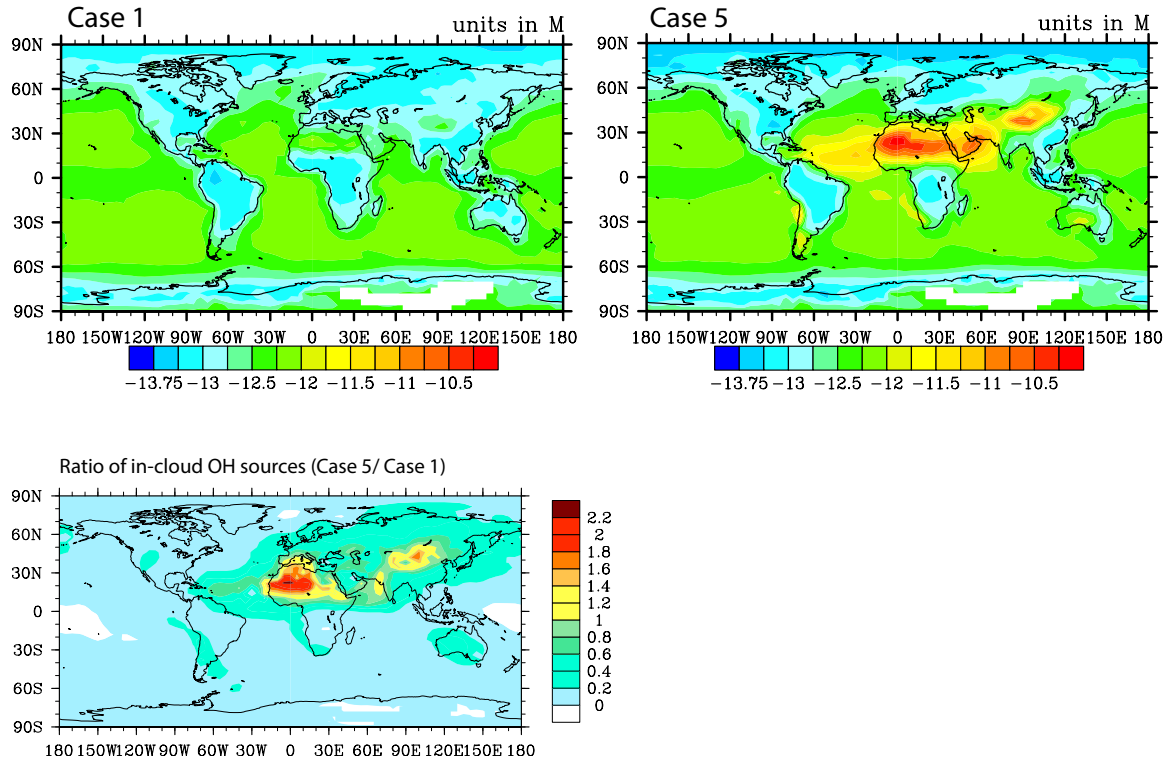


Figure 5. The predicted aqueous OH concentration (units in mol/L) in cloud water near 971 hPa in Case 1 (without Fe chemistry) and Case 5 (with Fe chemistry). The ratio of annual mean cloud water OH radical production rates in Case 5 to that in Case 1 is also shown (2nd row). The value shown is the logarithm of the ratio.

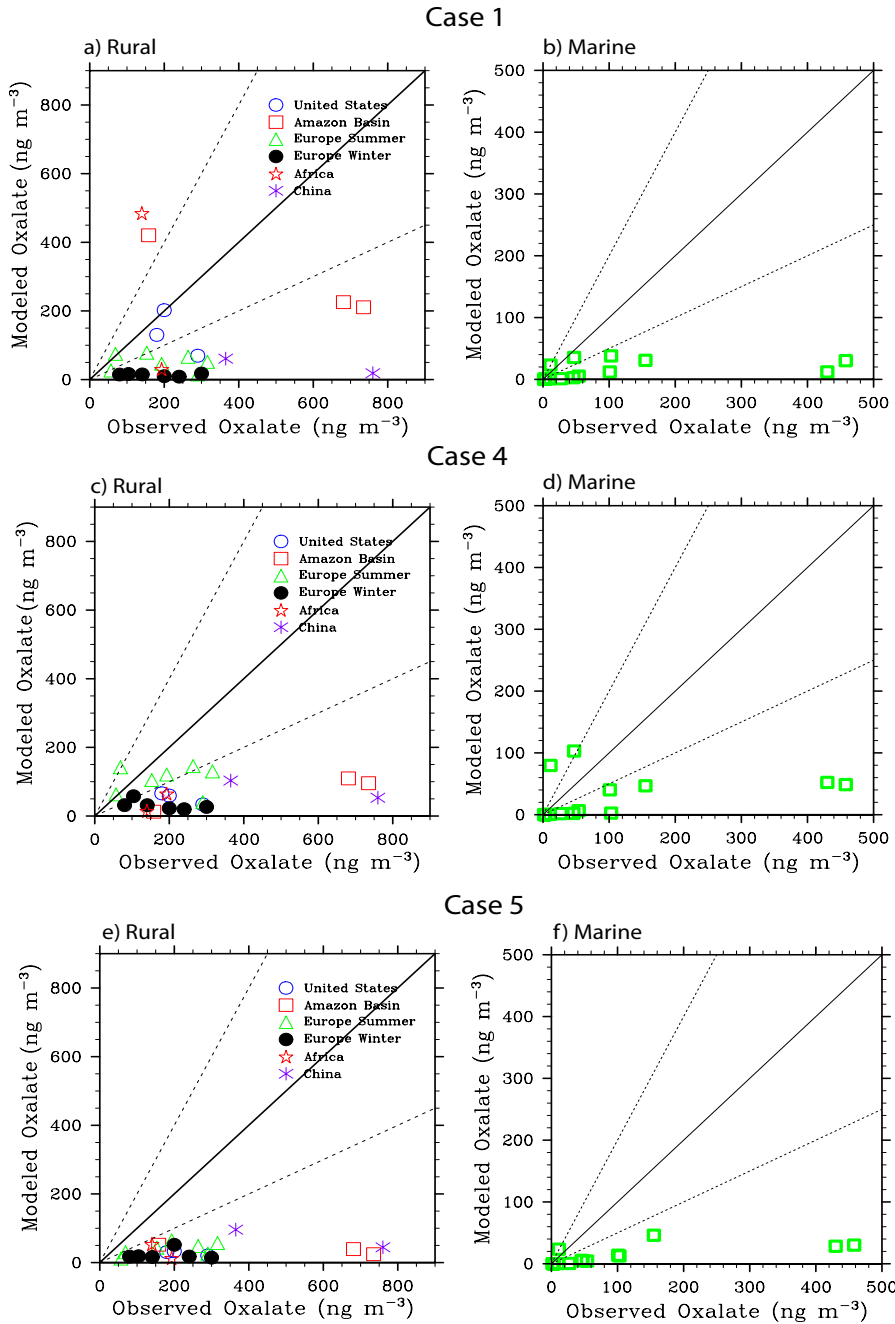


Figure 6. Comparison of the oxalate mass concentrations observed at rural and marine sites adopted from Table S3 of Myriokefalitakis et al. (2011) with the oxalic acid concentrations simulated in Case 1, Case 4 and Case 5. Solid lines show the 1:1 ratio, and dashed lines show the 1:2 and 2:1 ratios. The measurements at the various sites were made in different seasons and different years between 1980 and 2007 and most of them were reported with several days of sampling duration. The model results are the average values over the same months as the observations.

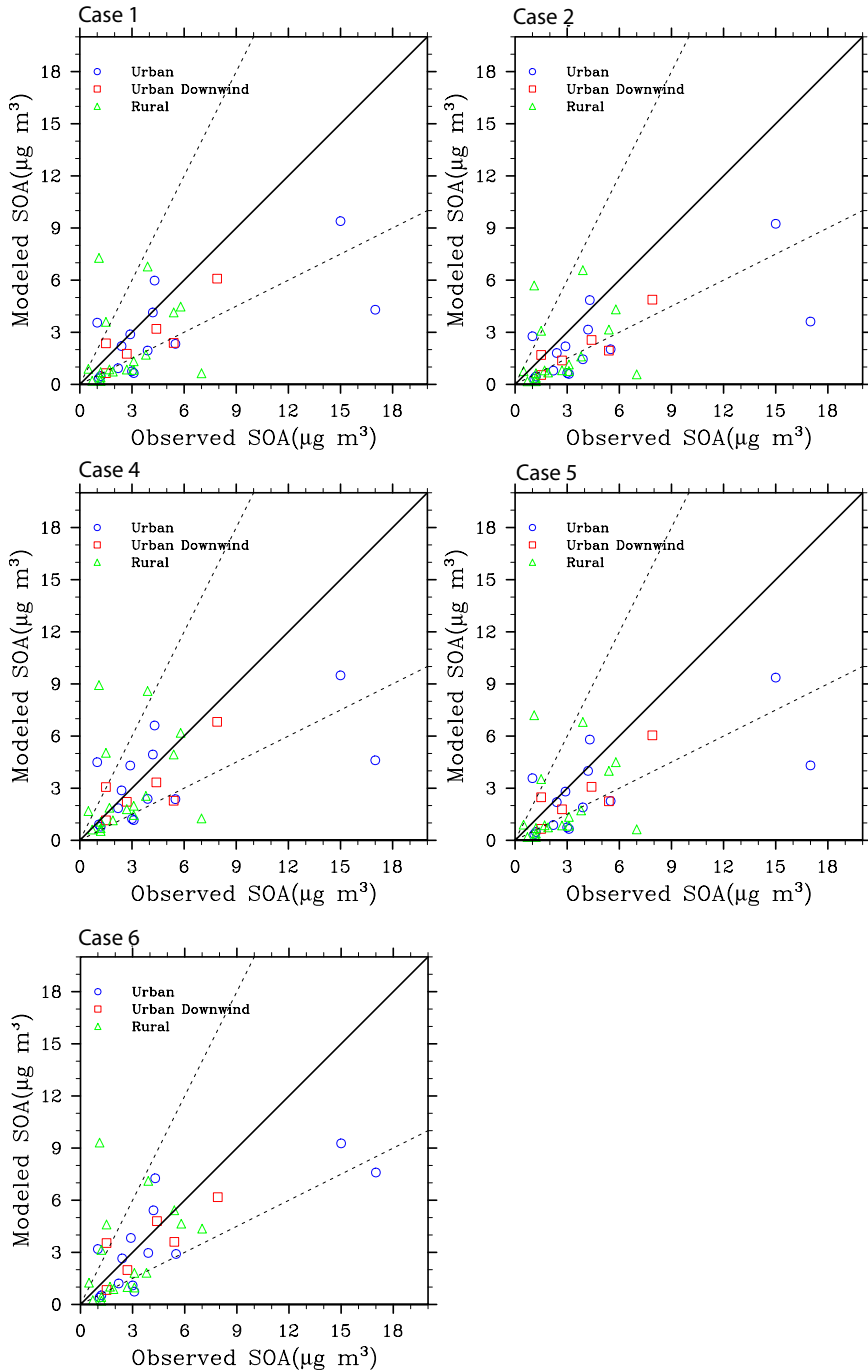


Figure 7. Comparison of SOA mass concentrations observed at the urban, urban-downwind and rural sites reported in Zhang et al. (2007) with those simulated in Case 1, Case 2, Case 4, Case 5 and Case 6. Solid lines show the 1:1 ratio, and dashed lines show the 1:2 and 2:1 ratios. The measurements at the various sites were made in different seasons and different years between 2000 and 2006 and were reported for the average of different durations spanning from 8 to 36 days. The model results are the average values over the same months as the observations.

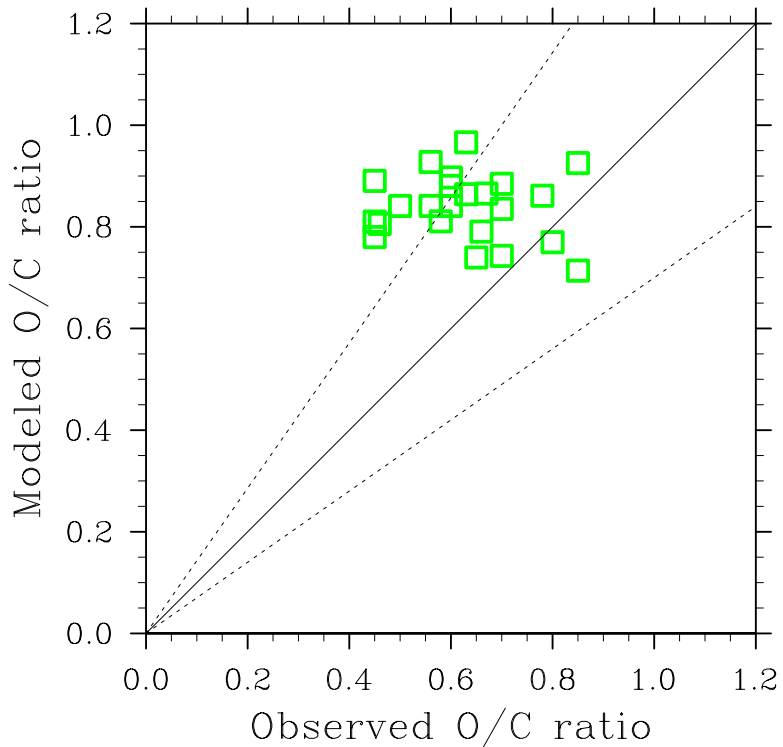


Figure 8. Comparison of O/C ratio estimated by Ng et al. (2010) for urban downwind, rural and remote sites with those simulated in Case 1. The values for other cases are similar to those in Case 1. Solid lines show the 1:1 ratio, and dashed lines show the 10:7 and 7:10 ratios, which roughly corresponds to the uncertainty of the AMS measurements, stated as 30% for the O/C ratio (Aiken et al. 2008). The measurements at the various sites were made in different seasons and different years between 2000 and 2009 and were reported for the average of different durations spanning from 8 to 36 days. The model results are the average values over the same months as the observations.